Shock effects in feldspars: an overview

Annemarie E. Pickersgill[1*], Steven Jaret[2], Lidia Pittarello[3,4], Jörg Fritz[5,6], and R. Scott Harris[7]

[1] School of Geographical & Earth Sciences, University of Glasgow, Gregory Building, Lilybank Gardens, Glasgow G12 8QQ, U.K.

[2] Department of Earth and Planetary Sciences, American Museum of Natural History, New York, NY 10024, U.S.A.

[3] Mineralogisch-Petrographische Abteilung, Naturhistorisches Museum Wien, Burgring 7, A-1010 Vienna, Austria

[4]Department of Lithospheric Research, University of Vienna, Althanstrasse 14, A-1090 Vienna, Austria

[5]Saalbau Weltraum Projekt, Liebigstraße 6, 64646 Heppenheim, Germany

[6]Zentrum für Rieskrater und Impaktforschung Nördlingen (ZERIN), Vordere Gerbergasse 3, 86720 Nördlingen, Germany

[7]Fernbank Science Center, 156 Heaton Park Drive, Atlanta GA 30307, U.S.A.

**Corresponding author. E-mail address: annemarie.pickersgill@glasgow.ac.uk (A. E. Pickersgill)*

ABSTRACT

Feldspars are the dominant mineral in the crust of most terrestrial planetary bodies, including Earth, Earth's moon, and Mars, as well as in asteroids, and thus in meteorites.

These bodies have experienced large numbers of hypervelocity impact events and so it is important to have a robust understanding of the effect that shock waves exert on feldspars. However, due to their optical complexity and susceptibility to weathering, feldspars are under-utilized as shock barometers and indicators of hypervelocity impact. Here, we provide an overview of the work done on shocked feldspars so far, in an effort to better frame the current strengths and weaknesses of different techniques, and to highlight some gaps in the literature.

1. INTRODUCTION

Hypervelocity impacts result in distinctive microstructural deformation in rocks and minerals during passage of a shock wave (e.g., French and Short, 1968; Roddy et al., 1978; Stöffler and Grieve, 2007; French and Koeberl, 2010). This shock metamorphism records the pressure, temperature, and strain rate conditions experienced by geo-materials during crater formation. Understanding the shock metamorphic overprint of planetary materials is crucial to the study of meteorites, terrestrial impact structures, and samples returned to Earth by space missions. Clear criteria for characterizing and quantifying the degree of shock metamorphism are required together with an understanding of how shock metamorphism affects different lithologies.

Shock metamorphic effects vary between rock types due differences in the mineralogy and microstructural characteristics of the target (e.g., French and Koeberl, 2010; Ferrière and Osinski, 2013 and references therein). This observation has been used to propose multiple shock classification schemes for different rock types including meteorites (e.g., Fritz et al., 2017), quartzofeldspathic rocks, sandstones, basaltic-gabbroic rocks, particulate rock material, chondritic and dunitic rocks (Stöffler et al., 2018). Shock effects are mineralogically selective, and heterogeneous in spatial distribution, such that neighbouring minerals, even if the same composition, may record different effects. This is due to differences in the shock impedance, a physical property of matter that describes how efficiently a shock wave propagates through a material. The mineral grains and pore spaces composing a polymineralic rock have different shock impedances, hence the shock wave propagates with variable efficiency, and this leads to a heterogeneous distribution of the maximum shock pressure and resultant shock metamorphic effects within a sample (e.g., Ogilvie et al., 2011). In addition, the degree and type of deformation is affected by the mineral's crystal structure and composition (Stöffler, 1972), pre-impact temperature (e.g., Langenhorst et al., 1992; Huffman et al., 1993; Langenhorst and Deutsch, 1994; Fritz et al., 2011) and pre-impact stress conditions (Daniel et al., 1997; Sims et al., 2019). Shock deformation of most minerals is evidenced by a progressive degradation of the crystal structure until melting occurs.

Feldspar group minerals (alkali feldspar and plagioclase) are both chemically and optically complex. Various publications address shock metamorphism for plagioclase, a major component in planetary materials, including asteroids, Mars, Earth, and Earth's moon. However, the K-rich alkali feldspars that are rare in meteorites but abundant in terrestrial rocks, have not been studied in as much detail. Feldspar group minerals suffer from alteration in a hydrous environment rendering them challenging to study using solely optical microscopy. Additionally, pre-existing microstructures, such as twin planes, cleavage planes, and exsolution lamellae, might be masking or possibly even precluding the formation of shock-generated planar features. The aforementioned challenges to studying feldspar microstructures coupled with inconsistencies in the features associated with different shock levels in different rock types (e.g., Stöffler et al., 2018; Fritz et al., 2017) make the utility of feldspars as a shock thermo-barometer variable.

Despite their abundance in rocky planetary materials, feldspars have been under-utilized for shock barometry compared to quartz and olivine. However, feldspar is becoming increasingly popular for shock barometry (e.g., Jaret et al., 2014; Kayama et al., 2018; Fritz et al., 2019a). In this paper, we discuss all impact cratering related effects on the feldspar group, but the reader should note that only definitive planar deformation features (PDFs), and diaplectic glass are considered *diagnostic shock effects* on their own (French and Koeberl, 2010). Certain high-pressure polymorphs can also be diagnostic, but only given a proper geologic context. Diagnostic shock effects are those that only form via passage of a shock wave with a strain rate and a pressure-temperature-time (P-T-t) path that cannot be produced by endogenic processes. Additional microstructures can form during impact cratering events but can also form by other geological processes. For example, fractures, kink bands, mosaicism, and darkening can inform the degree to which feldspars have been shocked, but these features can also be produced endogenically. Even tectonically-induced amorphization is possible, although only under extreme and rare conditions such as those reported for silica by Janssen et al. (2010).

2. Feldspar Group Minerals

Feldspars are the most abundant mineral group in crustal rocks on Earth (Deer et al., 2001), as well as in the crustal rocks of terrestrial planetary bodies (Papike et al., 1991). The feldspar group is composed of two solid solutions: alkali feldspar ($NaAlSi_3O_8$-$KAlSi_3O_8$) with a density of 2.62 - 2.55 g/cm^3 and plagioclase feldspar ($NaAlSi_3O_8$-$CaAl_2Si_2O_8$) with a density of 2.62 - 2.76 g/cm^3. Intergrowths of alkali and plagioclase feldspars are common, such as perthite (albite lamellae in K-feldspar host) and antiperthite (K-feldspar lamellae in albite). The crystal system is triclinic or monoclinic, depending on composition, thermal history, and crystallization temperature. Planar microstructures that are common in feldspar are good cleavage ({001} and

{010}) and the formation of twins (Seifert, 1964; Zoltai and Stout, 1984; Xu et al., 2016 and references therein). Common twins in alkali-feldspar are Carlsbad, with the z-axis as twin axis, and Baveno, with (021) as twin axis, and a combination of albite and pericline twinning, resembling a "tartan" pattern (Deer et al., 2001).

On planetary bodies with active hydrospheres, plagioclase routinely alters to sericite, zeolites, or clay group minerals. These products can locally be replaced by secondary calcite, due to hydrothermal alteration (e.g. Leichmann et al., 2003; Pittarello et al., 2013). A typical product of hydrothermal alteration of plagioclase is “saussurite”, an old term used to indicate a mixture of zoisite, epidote, sericite, and other components.

3. Shock effects in Feldspars

Shocked feldspar from impact structures on Earth, meteorites, and shock recovery experiments displays a range of shock-induced microstructures including undulatory extinction, mosaicism, planar microstructures, diaplectic glass, and melted (i.e., flow-textured and/or vesiculated) feldspar glass (Table 1, e.g., Stöffler, 1967; Stöffler et al., 2018). These effects result from progressive breakdown of the crystal lattice, and are linked with a specific range of shock pressures, temperatures, and anorthite content, as determined by high-pressure experiments (Fig. 1).

The state of matter under shock compression can be described with Hugoniot curves (e.g., Melosh, 1989; Langenhorst, 2002; Langenhorst and Deutsch, 2012; Fritz et al., 2017), which are depicted, for a specific mineral, in a density (or specific volume) vs. pressure plot. Figure 2 shows experimental data on anorthosite (rock composed mainly of Ca-rich plagioclase) derived from particle and shock wave velocity measurements at given shock pressures, with the specific volume calculated via the Rankine-Hugoniot relations. The Hugoniot is not a representation of a gradual increase in pressure and density, but describes the possible states achieved by a material that discontinuously jumps across the shock front from the uncompressed to the compressed state. The Hugoniot Elastic Limit (HEL) of a material indicates the transition from a purely elastic state to an elastic-plastic state. For feldspars, the HEL has been measured at 3.5-4.5 GPa. Pressures in excess of this range cause permanent changes in feldspar crystal structures (Ahrens et al., 1973; Grady and Murri, 1976; Huffman and Reimold, 1996). In addition, the Hugoniot of feldspar is subdivided into Regions I to III, which mark pressures above which the compressibility of the material during shock changes substantially. These regions correspond to specific shock metamorphic effects – the physical manifestation of the pressure-volume work during shock. Hence, shock effects from fracturing, kinking, and mosaicism, to formation of planar microstructures, diaplectic glass, and melting can be linked to a range of shock pressures. In order to appropriately extrapolate a shock pressure estimate to the whole rock, one must consider numerous grains throughout the sample, ideally in a variety of minerals. In the following sections, we provide an overview of the effects produced in feldspars during hypervelocity impact, both diagnostic (unique to impact) and non-diagnostic (formed both during impact and endogenically).

3.1. Fracturing

Fracturing is pervasive in rocks affected by impact (Fig. 3). The density of impact-induced fractures in quartz and feldspars has been found to increase with increasing pressure up to ~20 GPa (Lambert 1979). However fracture density decreases as pressure increases above ~20 GPa. Lambert (1979) concluded that the correlation between fracture density and pressure was too weak to be used for quantitative pressure calibration. Fractures are rare or absent in partly or fully isotropic feldspars (see Section 3.7).

3.2. Undulatory extinction

Undulatory (or undulose) extinction is the optical effect of a wave of extinction sweeping through a single crystal as the microscope stage is rotated with the sample between crossed polarizers; i.e., the entire crystal does not go in and out of extinction simultaneously (Fig. 4). This optical effect is the result of bending of the crystal structure without fracturing. Undulatory extinction is a common effect in minerals that have experienced non-uniform strain, and is not diagnostic of shock metamorphism, however it can be informative. For example, the amount of stress that a crystal has experienced can be qualitatively estimated based on how undulatory the extinction is; i.e., approximately how much variation in extinction angle is displayed within a single crystal? A higher amount of variation records higher strain. There is potential to quantify this effect using a Universal stage (U-stage) or electron backscatter diffraction (EBSD) measurements of the misorientation of the optic axes, however, we are not aware of any systematic studies attempting to quantify undulatory extinction in feldspars. Such efforts would be unlikely to develop a robust correlation given the ubiquitous nature of undulatory extinction as a result of tectonic deformation ($P \ll 1$ GPa).

3.3. Optical Mosaicism

Optical mosaicism is an extinction pattern observed in crystals composed of numerous subdomains, with differently oriented optic axes (e.g., Dachille et al., 1968; Stöffler, 1972; Stöffler and Langenhorst, 1994; French and Koeberl, 2010). This extinction pattern is different from undulatory extinction in which extinction passes smoothly through the crystal during rotation of the microscope stage. In mosaicism, subdomains are only a few micrometers in size, hence several rotated subdomains overlap in a typical ~30 μm thick thin section. Mosaicism is best observed in transmitted light between crossed polarizers, where it appears as a patchwork of extinction domains; with EBSD, as a patchwork of crystallographic orientations; or with single-crystal or in situ X-ray diffraction (XRD), producing arcs of diffraction spots instead of single spots. A similar pattern of extinction is also caused by endogenic processes (e.g., Spry, 1969; Vernon, 1975), so optical mosaicism cannot be used as a unique diagnostic indicator of shock metamorphism.

3.4. Planar microstructures

Shock related planar microstructures in feldspars include planar fractures (PFs), planar deformation features (PDFs), deformation bands, and kink bands (e.g., Stöffler, 1967, 1972; French and Short, 1968; French, 1998). PFs and PDFs in feldspar are not as well characterized as those in quartz, so we start with a brief discussion of these features in quartz to frame the discussion. In quartz, PFs are open cracks, typically >3 μm wide, and spaced ~15-20 μm apart; PDFs are lamellae composed of amorphous (or recrystallized) SiO_2, < 2 μm wide, and spaced ~2-10 μm apart (e.g., Engelhardt and Bertsch, 1969; Stöffler and Langenhorst, 1994; Langenhorst, 2002). Both PFs and PDFs are planar and form parallel to rational crystallographic orientations (French and Short, 1968; French et al., 2004).

Early reports of what are now referred to as PDFs in feldspar were described as various types of lamellae in plagioclase by both Stöffler (1967) and Dworak (1969). Stöffler (1967) described 1-8 μm thick isotropic (or low birefringence) lamellae spaced a few micrometers apart, similar to planar features described in quartz. Dworak (1969) described several types of lamellae, equivalent to deformation bands, PDFs, and PFs. The lamellae described as being most similar to quartz PDFs are 2-5 µm thick isotropic (or low birefringence) lamellae spaced about 10 µm apart, sometimes decorated with small inclusions. Dworak (1969) described feldspar PFs as up to 10 µm wide open fractures spaced a few micrometers apart and forming preferentially at grain margins.

In feldspar, PDFs occurring along with more widely spaced features (i.e., deformation bands or twins) form a ladder texture (Fig. 5) (e.g., Stöffler, 1967, 1972; Engelhardt and Stöffler, 1968; French and Short, 1968). Pittarello et al. (2013) reported microstructures in plagioclase that resemble feather features (FFs) previously described for quartz (Poelchau and Kenkmann, 2001), however no systematic study has yet been conducted on apparent FFs in feldspars. Sets of thin alternating isotropic lamellae (<10 µm wide) oriented parallel to the most common plagioclase twins have been reported as shock-induced microtwins (e.g., Stöffler, 1966; Dworak, 1969; Stöffler, 1972), though it has yet to be confirmed whether the formation of the microtwins is due to shock metamorphism, nor whether the currently isotropic lamellae originated as twin lamellae.

A great many planar microstructures exist in feldspars to begin with, so using an optical microscope alone to fully characterize putative PDFs is challenging, and it is better combined with high-resolution techniques such as electron microscopy. Pickersgill et al. (2017) investigated planar microstructures in Or-rich alkali feldspar from granitoid rocks from the Chicxulub impact structure using EBSD combined with transmission electron microscopy (TEM). EBSD highlighted semi-planar microstructures visible in transmitted light parallel to the trace of {001}, {010}, and {100}. Follow up TEM work revealed that the “planes” are in fact semi-coherent subgrain boundaries that are neither straight nor parallel (spacing varies from 0.2-0.6 µm between adjacent boundaries), and have no indication of amorphous material, making these subplanar microstructures distinct from the strict definition of PDFs as defined in quartz. The microstructures parallel to {110} form lamellar subgrains that, despite resembling strain-induced twins, are too closely spaced and narrow to be twins. Likewise, they are not exsolution lamellae as they show no chemical variation. Pittarello et al. (2020a) conducted EBSD on shocked plagioclase grains in a meta-granite from the Manicouagan impact structure, Canada. Results suggest that amorphization in plagioclase begins either within pre-shock twins or along shock-induced lamellae that are similar to both PDFs and micro-twins, likely representing structural failure of specific crystallographic planes during shock. Attempted indexing of these features using EBSD and U-stage resulted in orientations of {001}, {010}, and $\{1\bar{2}0\}$ or $\{1\bar{3}0\}$ (ambiguous).

PDFs in feldspars and quartz are reported to start to form at about the same pressure (>8 GPa, Stöffler, 1971; Ostertag, 1983), and are no longer present in samples subjected to pressures high enough to cause amorphization of the mineral (24-35 GPa). PDFs in feldspars have been reported for various impact structures including Ries (Stöffler, 1966; Engelhardt and Stöffler, 1968); Sudbury (French, 1968); Manicouagan (Dworak, 1969; Dressler, 1990; White, 1993); Gardnos (French et al., 1997); Tenoumer (French et al., 1970; Jaret et al., 2014); Dhala (Pati et al., 2010); and El'gygytgyn (Pittarello et al., 2013). Overwhelmingly, these are noted in passing as an accessory to PDFs in quartz, with rare attention or detail given to the PDFs in feldspar. As a result, the compositional range of feldspars bearing PDFs are rarely noted, but from the limited examples, PDFs appear to be confined to alkali feldspar or low-Ca ($<An_{\sim 50}$) plagioclase (Langenhorst et al., 1995; Trepmann et al., 2003; Gibson and Reimold, 2005; Nagy et al., 2008; Pittarello et al., 2013; Jaret et al., 2018), and are generally absent in higher Ca-plagioclase even for samples in shock ranges expected to form PDFs. For example, at the Mistastin Lake impact

structure, PDFs are abundant in quartz, and completely absent in plagioclase (An_{31-55}) (Pickersgill et al., 2015b). Similarly, at the Lonar Crater, India, which is a basaltic target with highly calcic plagioclase, no PDFs have been identified despite abundant examples of diaplectic glass (Kieffer et al., 1976; Jaret et al., 2015). However, we are aware of two exceptions to the high-Ca plagioclase resistance to PDFs, both in lunar anorthite, from the meteorite Oued Awlitis 001 (Wittmann et al., 2019), and Apollo sample 10046 (Dence et al., 1970). This indicates a strong compositional (and therefore crystallographic) effect on whether or not PDFs form in feldspars. The lack of observed planar features in experimentally shocked plagioclase (An_{63}) led Gibbons and Ahrens (1977) to suggest that the presence of PDFs in plagioclase is not as diagnostic of shock as maskelynite, and that PDFs would represent a purely local effect.

3.5. Shock darkening

Shock darkening is a reduction in the transparency of a mineral in transmitted light (e.g., Reimold and Miller, 1989; French et al., 1997; Jaret et al., 2018). This optical phenomenon is a common shock feature in mafic silicates, but has also been observed in feldspars (Fig. 6). Shock darkening of silicates is attributed to submicroscopic Fe-bearing droplets, that are mobilized and concentrated at shock conditions prior to melting (e.g., Rubin, 1992; Moreau et al., 2017). Shock darkening has been described in terrestrial shocked feldspars at the Gardnos (French et al., 1997), Manson (Koeberl et al., 1996), Roter Kamm (Reimold and Miller, 1989), and Sudbury (French, 1968) impact structures. Shock darkening has also been observed in experimentally shocked andesine, albite, and bytownite (Jaret et al., 2018). In plane-polarized light samples shocked between 17 and 50 GPa all show a pronounced darkening that is inherent to the samples and not a surface coating, nor does it correspond to elemental composition at the spatial resolution of the electron microprobe, which supports the attribution of darkening to submicrometer Fe-droplets. To our knowledge no atomic level study of shock darkened feldspars has been conducted. This effect is superficially similar to clouded feldspar, but can be differentiated in that in clouded feldspar the features are usually resolvable with an optical microscope (e.g., Poldervaart and Gilkey, 1954; Whitney, 1972; Smith and Brown, 1988; Putnis et al., 2007).

3.6. Alternate twin deformation

An effect observed in some feldspars is the deformation of only alternate twins in, for example, a polysynthetically twinned plagioclase. This alternate twin deformation includes the formation of possible PDFs in every other twin (forming a ladder texture or alternate twin lamellae, Fig. 5a,b), and the formation of diaplectic glass (alternate twin isotropisation). Alternate twin effects are interpreted to occur in response to "favorable" crystallographic orientation of one twin set with respect to the local shock wave (Stöffler, 1966, 1967; Taylor and Dence, 1969; Robertson, 1973; Dressler, 1990; Jaret et al., 2014; Pickersgill et al., 2015b; Pittarello et al., 2020a). Jaret et al. (2014) interpreted alternate twin deformation to indicate relatively low pressure conditions where subtle orientation differences are enough to impede shock deformation, whereas at higher shock conditions there is so much energy that slight misorientations do not affect the deformation process. Likewise, Pickersgill et al., (2015a) used in situ micro X-ray diffraction (μXRD) to find that adjacent twin sets generally deform to the same degree, which they interpreted to mean that the difference in lattice orientation between twins relative to the shock wave that causes alternate twin deformation occurs over a very narrow range of orientations.

3.7. Diaplectic glass

Diaplectic glasses, sometimes (in older papers) referred to as *thetomorphic glasses*, are phases which are optically isotropic (i.e., extinct on rotation of the stage between crossed polarisers); amorphous to Raman, X-ray diffraction, or other techniques that measure crystallinity; but still retain the exact chemical composition, and morphology of the precursor mineral thereby preserving the original rock fabric (Fig. 7) (e.g., Engelhardt et al., 1967; Binns, 1967; Engelhardt and Stöffler, 1968; Hörz and Quaide, 1973). Diaplectic glasses do not exhibit flow textures or vesiculation, even when observed using high resolution imaging techniques such as scanning electron microscopy (SEM). Preservation of the internal fabric is indicated by preservation of, for example, magmatic pyroxene lamellae in maskelynite from the Martian meteorite Shergotty (Fig. 7) and Fe-oxide "clouding" in diaplectic plagioclase glass from the Mistastin Lake impact structure (Pickersgill et al., 2015b). Even chemical zonation is preserved in diaplectic plagioclase glass from both terrestrial impact structures (Jaret et al., 2015) and meteorites (Treiman and Treado, 1998). The transition from crystalline (i.e., birefringent) feldspar to diaplectic feldspar glass is documented by grains in which some areas are amorphous, and some areas remain birefringent. This transition can manifest as alternate twin isotropisation (Stöffler, 1966, 1971; French, 1998), but is equally found unrelated to twins or other planar features (Fig. 7C,D, e.g., Pickersgill et al., 2015b; Pittarello et al., 2020a, 2020b). Both partially and fully isotropic diaplectic glasses are characterized by a lack of fracturing, even when surrounded by highly fractured minerals (Fig. 7 a,b).

3.7.1. Identification

In transmitted light, initial suspicion of diaplectic glass comes from noting a grain that is constantly extinct between crossed polarizers. In reflected light or during SEM of a polished surface (thin or thick section), initial inference of diaplectic glass comes from observing a notable pattern of fractures: fractures are rare or absent in partly and fully isotropic feldspar and fractures in adjacent minerals such as olivine and pyroxene terminate at the interface with the diaplectic glass (see Fig. 7 a,b).

In order to definitively identify diaplectic glasses, it is crucial to ensure that the phase being examined is 1) amorphous, and 2) the same composition as feldspar. Permanent extinction under an optical microscope can indicate a) an amorphous phase; b) orientation of an optic axis of a crystal parallel to the line of sight of the microscope (perpendicular to the thin section surface); and c) naturally isotropic minerals (e.g., garnet). It is therefore necessary to confirm an amorphous state using additional techniques such as obtaining an interference figure using the Bertrand lens of the microscope (no interference figure should be present with an amorphous phase), or using a U-stage to rotate the sample out of extinction. If the phase is indeed amorphous, in situ μXRD will reveal a diffuse band across the detector rather than distinct diffraction spots. Likewise, Raman spectra of amorphous feldspar have two broad peaks of relatively low intensities at ~400-600 Δ cm^{-1} and ~1000-1100 Δ cm^{-1} (Fig 14). Composition should be confirmed using an analytical SEM or electron probe microanalysis (EPMA).

3.7.2. Structure

The amorphous nature of diaplectic glasses suggests that they have lost the ordered internal atomic arrangement of the precursor crystal. However, diaplectic feldspar glasses display several properties that indicate a transitional state between a crystal and a glass produced by quenching of a molten mineral (i.e., a monomineralic melt glass):

1) Diaplectic plagioclase glass has a density and refractive index (RI) intermediate between a plagioclase crystal and a melt glass of identical chemical composition (Engelhardt et al.

1967;Ostertag 1983; Fritz et al. 2019a). Both density and RI decrease with increasing shock level (Arndt et al., 1982, see Fig. 8);

2) Diaplectic glasses maintain substantial intermediate-range structural order, unlike melt glasses (e.g., Milton and de Carli, 1963; Bunch et al., 1967; Arndt et al., 1982; Ostertag, 1983; Jaret et al. 2015).

3) Diaplectic plagioclase glass retains a structural memory of its former crystalline state (Milton and de Carli, 1963; Bunch et al., 1967; Hörz and Quaide, 1973; Arndt et al., 1982; Diemann and Arndt, 1984; Jaret et al., 2015).

When heated at ambient pressure, diaplectic glasses can recrystallize back into a single crystal, which is distinctly different from melt glass, which always reverts to a polycrystalline aggregate (Bunch et al., 1967; Arndt et al., 1982). Sometimes these recrystallized feldspars even regain undulatory extinction. Further investigations into the memory effects of diaplectic glass have been investigated using high-pressure experiments and are discussed in Section 4.

Structural differences between melt glass and diaplectic glass have been investigated by a number of techniques. Synchrotron X-ray total scattering experiments of crystalline plagioclase, natural diaplectic plagioclase glass, and fused plagioclase glass (all of labradorite composition) show that both glasses are characterized by lack of periodicity beyond distances of 10 Å, unlike crystalline plagioclase (Jaret et al., 2015). However, in the intermediate range (4–10 Å) the diaplectic glasses show a higher degree of atomic order than melt glasses (Jaret et al., 2015). Orientation sensitive measurements on diaplectic glass have suggested retention of orientation and position of some atoms despite loss of long-range order. Micro-FTIR spectroscopy of individual naturally and experimentally shocked plagioclase grains is also sensitive to orientation, where peak positions and intensities of vibrational modes in plagioclase can shift by ~40 wavenumbers, making it difficult to correlate changes in peak intensities or positions with shock level (Fig. 9). However, the degree to which orientation affects the spectra decreases with increasing shock level (Jaret et al., 2015). Orientation effects have been found to be a useful tool for distinguishing between diaplectic and melt-produced glasses. For example, in infrared spectroscopy diaplectic labradorite glass exhibits one Si-O stretching band, but this peak position changes by 40 wavenumbers upon rotation of the grain (Fig. 9). Melt glass on the other hand does not show effects of orientation on spectral position (Jaret et al., 2015). Nuclear magnetic resonance (NMR) spectroscopy shows the overall spectral shape and pattern of diaplectic labradorite glass is similar to that of crystalline plagioclase, suggesting a lack of large-scale differences in structure or silica polymerization. Fused labradorite glass on the other hand has a larger difference in chemical shift in NMR spectra compared to crystalline labradorite, further supporting that diaplectic plagioclase glass and fused plagioclase glass are structurally different (Jaret et al., 2015).

3.7.3. Alteration

In a hydrous environment, feldspars and diaplectic glass are susceptible to alteration. As a result, recrystallized feldspars are typical in terrestrial impactites. The resultant textures are described as spherulitic or plumose microcrystals, interpreted as evidence of altered diaplectic glasses during post-shock heating (French, 1998). This effect occurs in the Manson impact structure, where shocked plagioclase appears to have highly altered alternating twins (Short and Gold, 1996). Likewise, at the Mistastin Lake impact structure, alternating twins in some samples have altered to zeolites (Pickersgill et al., 2015b). In both cases, these textures are interpreted as preferential alteration of diaplectic glass in grains that underwent alternate twin isotropization.

3.7.4. Formation pressure

Fully isotropic diaplectic feldspar glass forms by the passage of a shock wave with pressures of more than 24-30 GPa and less than ~47 GPa (Table 1, Ostertag, 1983; Jaret et al., 2018; Fritz et al., 2019a). Both meteorites and terrestrial impactites have documented a relationship between the formation of diaplectic plagioclase glass from plagioclase in contact with shock melt veins (Walton et al., 2016; Sharp et al., 2019). In these cases, plagioclase further from melt veins, or in contact with thin (1-4 μm) veins remains crystalline, but plagioclase in contact with melt veins has become isotropic. The formation of diaplectic glass is therefore attributed to the elevated temperature gradient caused by contact with shock melt, combined with the large deviatoric stresses experienced by minerals along vein margins. These natural observations agree with experimental results that demonstrate that both elevated temperature and shear stress reduce the pressure at which plagioclase transforms to diaplectic glass (e.g., Kubo et al., 2010; Daniel et al., 1997). There is a strong compositional effect on the pressures associated with amorphization, where more calcic plagioclase becomes amorphous at lower pressure conditions (Ostertag, 1983; Angel, 1994; Fritz et al., 2019a; Jaret et al., 2018). Most likely this trend reflects the Si-Al polymerization rather than Ca content directly (Angel, 1994; Jaret et al., 2018). There has been significantly less work on quantifying the differences in shock response between the alkali-series feldspars. Ostertag (1983) reported amorphization of experimentally shocked sanidine and orthoclase at pressures of ~30 and ~32 GPa, whereas microcline retained some birefringence up to pressures of 45 GPa.

The transitional regime between diaplectic and melt glasses results in shock-temperatures in plagioclase that are not high enough to cause melting of the whole grain, but are just high enough to cause eutectic melting along plagioclase/pyroxene interfaces (Fig. 7) and assimilation of minerals with a lower melting point.

3.8. Melting

At higher shock pressure monomineralic melt glass forms with the same composition as the original feldspar (e.g., Stöffler, 1972, 1967). An example of fully melted plagioclase glass is shown in Fig. 10, in the strongly shocked Martian meteorite ALH 77005. Petrographically melted feldspar glass is significantly different from diaplectic feldspar glass in that melt glass displays flow textures and/or vesicles.

Upon cooling, if the pressure pulse is longer than the undercooling, high pressure phases can crystallize from the melt (e.g., Sharp and DeCarli, 2006; Walton et al., 2014). Small occurrences of plagioclase-composition melt glass can be identified by careful high-resolution backscatter electron imaging (El Goresy et al., 2013). Care must be taken to ensure that apparent feldspar-composition glasses are not whole-rock melts using EPMA or analytical SEM. Feldspar melting is associated with local peak shock pressure of ~ 45-50 GPa, however melting can occur in porous targets shocked to lower pressures, where the shock kinetic energy is mostly converted into heat (e.g., Kieffer, 1971; Davison et al., 2010).

3.9. High pressure polymorphs

The temperatures during shock are such that weakly to strongly shocked rocks can serve as a heat sink allowing localized zones of shock melt to quickly cool by assimilation and thermal conduction during elevated shock pressure conditions. Therefore, localized zones of shock melt (10s to 100s of micrometers in size) provide the pressure-temperature-time path (P-T-t) allowing for the formation and preservation of a variety of high-pressure phases (Tomioka and Miyahara, 2017; Fritz et al., 2017). These local zones of shock melt serve as natural crucibles mimicking the conditions in the Earth's lower crust or mantle. High-pressure minerals are not common in Earth's upper crust, but they are produced endogenically and therefore can only be related to shock when observations are combined with relevant geologic context (French and Koeberl, 2010). A list of high-pressure minerals related to shocked feldspar is given in Table 2, together with their chemical formulae, experimentally derived pressure and temperature (P-T) stability fields and references. High-pressure phases have been identified in most types of meteorites, in various rocks from terrestrial impact structures, and synthesized in high-pressure laboratory experiments. This indicates that formation and preservation of high-pressure phases is a typical result of impact cratering events.

3.10. Sieve-texture and checkerboard feldspar

"Checkerboard" feldspar is a checkered-looking pattern of subgrain domains found within feldspar clasts in impact melt rocks (Fig. 11). Checkerboard texture has the appearance of crystallographically controlled individual rectangular domains separated by melt products (e.g., Grieve, 1975). Internal features such as twinning and extinction angle are preserved across the grains demonstrating that they were once a single crystal (Fig. 11). This texture was originally termed "checkerboard" by Grieve (1975), who described unshocked partly digested plagioclase inclusions in a melt rock with a sieved, "checker-board" appearance due to thermal effects of the surrounding melt. Bischoff and Stöffler (1984) first proposed a detailed scenario for development of sieve texture in clasts in impact melt rock from the Lappajärvi impact structure (Finland). Their scenario essentially regarded checkerboard texture as the result of rapid, crystallographically-controlled recrystallization from diaplectic feldspar glass, comparable to the suggested formation of ballen quartz (e.g., Ferrière et al., 2010). As such, the texture would represent positive evidence of transient shock pressures exceeding 25-35 GPa.

Whitehead et al., (2002) revised the formation of checkerboard texture based on feldspar clasts in melt rocks from the Popigai impact structure. Their scenario more closely resembles the disequilibrium melting of plagioclase observed during the rapid decompression of intermediate composition magmatic systems, resulting in typical (i.e., igneous) "sieve-textured" feldspar (Nelson and Montana, 1992). Whitehead et al. (2002) noted similar textures in clinopyroxenes in the Popigai impact melt rocks, which are also commonly associated with so-called "sieve-textured" feldspars in volcanic rocks.

A texture similar to checkerboard feldspar occurs in volcanic rocks, and is also referred to as "sieve texture". The images that accompany the igneous definition of "sieve texture" (Klein and Philpotts, 2016) imply crystallographic control of the melt channels. This can lead to confusion when the terms "sieve-texture" and "checkerboard texture" are used interchangeably, because there are two genetic interpretations for a similar appearance: i) volcanic chemically driven disequilibrium melting (Nelson and Montana, 1992) and ii) impact-induced crystallographically controlled disequilibrium melting (Whitehead et al., 2002).

Whitehead et al., (2002) attempted to distinguish impact melting from igneous melting based on the optical crystallography and X-ray element mapping of subgrains within the feldspar clasts. However, it is not clear from their observations that distinguishing these two processes is possible (Harris et al., 2019). Therefore, it has not been convincingly shown that the sieve texture of igneous petrologists and the sieve or checkerboard texture of impact petrologists are the result of different processes. Consequently checkerboard or sieve-texture feldspar, while common in both volcanic and impact melt rocks, should not be used as a unique diagnostic criterion of either process unless significant progress is made in differentiating igneous sieve texture from impact-induced sieve or checkerboard texture.

4. Experimental Shock Calibrations

High-pressure experiments enable formation conditions (i.e., pressure, temperature, timing) to be assigned to rock and mineral samples based on the microscopic textures produced. Such experiments are conducted using four main techniques: 1) shock experiments; 2) shock recovery experiments; 3) rapid compression experiments; 4) static compression experiments. These different techniques (1-4 in previous sentence, summarized in Table 3) create different physical conditions. As a result, the same high-pressure effects (e.g., amorphization) may develop at different pressure and temperature conditions depending on the experimental process and the characteristics of the test material (i.e., initial grain size, composition, porosity, presence of structural defects, etc.). Therefore, the reported experimental data need careful evaluation before comparing results between different experiments and their application to natural shock metamorphism. The experimental setups mentioned previously could influence the pressures at which specific microstructural deformation is observed in several ways:

1) By studying the samples in a compressed or decompressed state, i.e., in situ during static pressure experiments or after decompression to ambient pressure from static pressure experiments (Daniel et al., 1997; Johnson et al., 2002a, 2003; Kubo et al., 2010; Jaret et al., 2018).

2) By applying hydrostatic or non-hydrostatic conditions to the sample (Daniel et al., 1997)

3) By changing the rate at which the sample is compressed (e.g., Sims et al., 2020)

4) By changing the duration of the high-pressure conditions (Huffman et al., 1993; Kubo et al., 2010; Ogilvie et al., 2011; Fritz et al., 2019a); and,

5) By selecting the pre-experiment or the syn-experiment temperature of the experimental setup (Gratz et al., 1992; Huffman and Reimold, 1996; Kubo et al., 2010; Tomioka et al., 2010; Fritz et al., 2011, 2019a).

In addition, experimental measurements of the shock wave and particle velocity parameters allow for calculation of the pressure, density, and energy of the compressed material using the Rankine–Hugoniot relations (Fig. 2). These different experimental approaches have provided a variety of complementary information on material properties during shock compression and after decompression to ambient pressures (see Section 3).

The wealth of experimental data provides space for a variety of opinions among shock researchers. For simplicity, the discussion can be separated into two end-member interpretations:

1) *The shock metamorphic record in naturally shocked rocks is in conflict with experimental results obtained by the different types of experiments* (Stöffler et al., 1991, 2018; Chen et al., 1996; Sharp and DeCarli, 2006; Gillet et al., 2007; El Goresy et al., 2013). Various researchers agree that there is a substantial difference between results from static pressure and dynamic (shock) pressure experiments, with different authors favoring results from either one or the other (Stöffler and Langenhorst, 1994; Sharp and DeCarli, 2006; Gillet et al., 2007; Kubo et al., 2010; Jaret et al., 2018; Sims et al., 2020). The argument is that static experiments are too slow and do not generate a shock wave, because the pressure increases stepwise and is sustained over relatively long time scales of seconds to minutes. The dynamic experiments occur over extremely short timescales (~1 ns – 1 μs) and cannot sustain the shock conditions for the same duration as in a natural impact event. In the case of reverberation shock experiments, the maximum pressure is not achieved in a single shot as is the case in natural shock waves (Langenhorst, 2002). Thus, neither static

nor dynamic experiments reproduce the duration and loading path as inferred for the natural case (Stöffler and Langenhorst, 1994; Sharp and DeCarli, 2006; Gillet et al., 2007), which is typically in the temporal range of milliseconds to rarely a few seconds (Langenhorst, 2002; Sims et al., 2019; Bowling et al., 2020). These interpretations are due to a well-discussed discrepancy between the pressures associated with transformations observed in static experiments compared to those in dynamic experiments. For example, diamond anvil cell (DAC) experiments and shock experiments from the same starting material show a ~7-9 GPa difference in amorphization pressures (Jaret et al., 2018; Sims et al., 2020), consistent with interpretations compiled from literature of either isolated shock or static experiments (Daniel et al., 1997; Johnson et al., 2002a, 2003). Sims et al. (2020) recognized memory effects in the DAC experiments suggesting two amorphization points – one where the sample appears amorphous while still under compression, and a higher point where the sample remains amorphous after decompression. The higher pressure is closer to those of the shock experiments, which may in part help reconcile the discrepancies. Recent "rapid compression" experiments using membrane DAC setups that allow for control on strain-rate have shown that strain rate has a significant effect on the pressures at which plagioclase deforms (Sims et al., 2019).

2) *The shock metamorphic record in naturally shocked rocks agrees with the results obtained by both shock and static pressure experiments* (Fritz et al., 2017). Shock recovery experiments show that with increasing shock pressure different types of shock deformation effects develop in olivine and plagioclase, respectively. These two different thermo-barometers provide consistent results if studied in naturally shocked rocks such as shocked igneous Martian meteorites (Fritz et al., 2005a). These consistent results mean, that either both olivine and plagioclase are affected by potential differences between shock recovery experiments and the natural case to the same degree, or that shock recovery experiments accurately reproduce the conditions in a natural impact event. Shock reverberation experiments and hydrostatic pressure experiments produce an amorphous material from plagioclase and quartz as long as both types of experiments achieved the same pressure and temperature conditions and the samples are studied in a decompressed state (Fritz et al., 2019a). The shock-loading path achieved in shock

> reverberation experiments is a reasonable analog for the diffuse shock front traveling through lithological units composed of different types of minerals, porosity and fractures during a natural impact event (Fritz et al., 2011). Shock reverberation experiments allow well-defined shock pressures to be applied to a relatively large sample volume (Müller and Hornemann, 1969; Fritz et al., 2011). Most problems regarding the shock thermo-barometry of meteorites are not related to experimental limitations but mainly result from inconsistent interpretation of the observational evidence (Fritz et al., 2017, 2019a). This includes: a) Misunderstandings regarding the duration of isobaric shock pressure conditions in naturally shocked rocks, which mostly implies that high-pressure phases form in (and near) local shock melt zones during declining shock pressures, b) A mineralogically inconsistent definition of the S6 shock level leading to an incorrect shock pressure assignment of all chondrites containing high-pressure phases (Fritz et al., 2017).

Reconciling the different interpretations of the shock thermo-barometry of rocks remains an ongoing area of active research and discussion. For example, a recent study of the shock stage distribution of 2280 ordinary chondrites confirmed that all S6 chondrites need reclassification (Bischoff et al., 2019). Despite these discussions, there is agreement on the types of shock deformation effects in feldspar and the order in which these shock effects occur with increasing pressure (see Section 3).

5. Quantifying shock features in feldspars

Multiple techniques have been applied to begin to quantify shock effects in feldspars. These techniques are summarized in Table 4, and discussed in the following sections.

5.1. Measuring planar microstructures in feldspars

In quartz, the number and orientation of PDF sets have been correlated with specific pressures through shock loading experiments allowing for refined pressure estimates from measurement of PDF orientations (e.g., Hörz, 1968; Huffman and Reimold, 1996; Ferrière et al., 2009). Such a correlation has not been developed for feldspars due to the complexities involved in PDF formation, identification, and orientation measurement in this mineral group.

The universal stage (U-stage) is the most common method of determining PDF orientations in quartz, and this method has been used with feldspars, though it is significantly more challenging (Stöffler, 1967; Dworak, 1969; Pittarello et al., 2020a). Measuring the crystallographic orientation of any planar element in feldspars is complicated compared to measuring the same features in quartz because feldspar is optically biaxial, and the crystal structure (and therefore optical properties) of feldspars varies with composition through the solid solution from Ca-rich to Na-rich to K-rich end members (Doeglas, 1940; Haff, 1940; Fairbairn and Podolsky, 1951). Therefore in addition to the measurements themselves being complex, accurately indexing the measured planes requires use of the specific indexing template for the composition of feldspar under investigation; examples of such indexing templates can be found in Stöffler (1967) and Dworak (1969). These factors result in orientation measurements of planar features in feldspars using solely a U-stage to be both time-consuming and error-prone. For example, Dworak (1969) measured 113 lamellae in 51 crystals of labradorite using the U-stage, but due to the inherent difficulty in using a U-stage with feldspars, the lowered birefringence of some host crystals, and the changes in An content (even within a single zoned crystal) the assignment of the orientation of these lamellae had a large error. The most common PDF orientations measured in feldspars are summarized in Table 5. Both Stöffler (1967) and Robertson (1966) came to the conclusion that planar deformation features in feldspar form over such a narrow range of pressures that it would not make sense to correlate orientations with peak pressures. By implication, the mere presence of planar deformation features in feldspar, regardless of their orientation, would be a sensitive shock barometer.

An additional issue in investigating PDFs in feldspar with the U-stage is optimizing the choice of glass hemispheres. The glass hemispheres each have a fixed refractive index, and for accurate measurements the refractive index must be the same as the host crystal. However, the refractive index of plagioclase ranges from 1.53 (albite) to 1.59 (anorthite) and for K-rich feldspar, it ranges from 1.518 (orthoclase) and 1.539 (microcline). The hemispheres used for measurements in quartz have refractive index 1.554, which is between the end member values for plagioclase, but is too high for K-feldspar. Hemispheres with closer refractive indices exist, but are not readily available to order and are difficult to match to the grain of interest. However, the error induced by the difference in refractive index between the investigated grain and that of the glass hemisphere pair can be calculated, and used to correct the data (e.g., Reinhard, 1931).

To circumvent some of the difficulties encountered by using the U-stage alone, EBSD has recently been combined with U-stage or focused ion beam (FIB) milling and BSE imaging to measure orientation of PDFs. EBSD provides crystal orientation of the host mineral circumventing some of the challenges of defining a unique orientation to a biaxial mineral using the U-stage alone. EBSD can also be used to determine a family of planes to which the trace of a plane most likely belongs. However, to complete the orientation measurement in 3D, a "dip" measurement is acquired using the U-stage (Pittarello and Koeberl, 2017; Pittarello et al., 2020a, 2020c) or by making a FIB trench perpendicular to the trace of the plane and measuring the dip off the resultant image (Pickersgill and Lee, 2015). Thus far, using the FIB technique for this purpose has been demonstrated only for quartz, however the same principle should work for feldspars. Currently, transmission electron microscopy (TEM) is necessary for a definitive identification of the crystallographic orientation along which PDFs develop in feldspar.

5.2. Density, refractive index, and birefringence

Density, refractive index (RI), and birefringence decrease as pressure increases until the mineral becomes amorphous (Stöffler, 1974; Stöffler and Langenhorst, 1994). At shock pressures <20 GPa the RI of shocked crystalline (birefringent) feldspar is only slightly lower than the RI of unshocked feldspar (Kleeman, 1971; Stöffler, 1974; Robertson, 1975). At pressures greater than ~24 to 35 GPa (depending on chemical composition), feldspars are completely converted to an amorphous state (diaplectic glass). Once this has occurred, and for each type of feldspar over a very narrow pressure range, the RI of diaplectic feldspar glass drops sharply (Ostertag, 1983). Shock pressures of ~45 GPa produce an amorphous material with a RI matching that of a melt glass of identical chemical composition to feldspar. As an exception, diaplectic anorthite glass produced in 41.5 GPa shock experiments displayed a RI that was higher than that of unshocked crystalline anorthite (Fritz et al., 2019a). The well-tested relationship between the refractive index of diaplectic feldspar glass, the An content, and the shock pressure is illustrated in Figure 9 (e.g., Binns, 1967; Engelhardt et al., 1970; Stöffler et al., 1975; Robertson, 1975; Ostertag, 1982; Fritz et al., 2019a).

5.3. X-Ray Diffraction (XRD)

Two types of X-ray scattering experiments have been applied to shocked feldspars: X-ray diffraction (XRD) experiments by powder or single-crystal XRD, in situ μXRD (in thin section and hand sample), and high-energy total X-ray scattering experiments using a synchrotron. Contributions by total-scattering experiments are discussed in section 3 as they relate to amorphous phase studies. At pressures too low to induce amorphization or phase-change, XRD patterns show peak broadening. There are two types of peak that can broaden in this fashion, peaks in the chi direction (visible with single-crystal or μXRD) and peaks in the 2θ direction (visible with single-crystal, μXRD, and powder diffraction).

Shock experiments on andesine (4-10 GPa) and oligoclase (3-34 GPa) by Hörz and Quaide (1973), showed that the degree of crystal lattice damage is correlated with shock pressure. Furthermore, by using single crystal XRD to measure the length of streaks in the chi direction (i.e., strain-related mosaicity) they could start to quantify the amount of strain recorded by the crystals and use that as a proxy to quantify shock level. A correlation between streak length and shock level was also documented in a single-crystal XRD study of plagioclase from the Charlevoix impact structure (Walawender, 1977). Pickersgill et al. (2015a) built upon this work by using in situ μXRD to quantify strain-related mosaicity by measuring the full width at half maximum (FWHM) of the intensity vs. chi angle pattern, and compared those measurements to optical signs of shock in samples of labradorite and andesine from the Mistastin Lake impact structure, and lunar anorthite collected during the Apollo program. As with the single-crystal studies discussed previously, peak broadening in the chi dimension increased with increased optical signs of shock, up to amorphization of the sample (i.e., formation of diaplectic glass) – at which point the X-rays produced a diffuse band on the detector. Powder XRD analyses of shocked and unshocked sanidine by Kayama et al. (2012) reported almost no change in diffraction peak intensity between samples. However, with increased shock pressure they did find slight peak broadening in 2θ, followed by a sudden change to no detectable peaks (i.e., an amorphous pattern) for amorphous samples.

Strain-related mosaicity, as measured using in situ μXRD or single-crystal XRD, shows more variation in shock level of feldspars prior to amorphization than optical determinations, and likely could be useful in subdividing the lower end of the shock scale (Pickersgill et al., 2015a). However, in order to properly quantify shock via strain-related mosaicity, more work needs to be done such as correlating results with those from other techniques (Raman for example) and via application to a wider variety of feldspar compositions and, ideally, also to experimentally shocked samples. Caution must be applied when using XRD to measure shock, as the features described in the previous paragraphs indicate strain, and therefore, without contextual information, it is impossible to differentiate the cause of the strain (i.e., shock or tectonism).

5.4. Thermal Infrared Absorption Spectroscopy

Thermal infrared absorption spectra of naturally shocked feldspars show lower intensity and less spectral detail than unshocked feldspar. Both detail and intensity continue to decrease as pressure increases as a result of increased glass content and progressive lattice disordering (Lyon, 1963; Bunch et al., 1967; Stöffler and Hornemann, 1972; Stöffler, 1974; Arndt et al., 1982; Ostertag, 1983; Johnson et al., 2002b, 2003; Jaret et al., 2015, 2018). Crystalline feldspars exhibit infrared reflectance peaks between 950 and 1150 cm^{-1} (reststrahlen bands) that correspond to Si-O stretching modes of the SiO_4 tetrahedra. Additional peaks occur between 700 and 850 cm^{-1} corresponding to Si-bridging oxygen modes, and between 400 and 600 cm^{-1} corresponding to O-Si-O bending modes (Iiishi et al., 1971; Okuno, 2003). Bulk IR emissivity of experimentally shocked albite shows a progression of change to the IR spectra in the form of decrease in overall band intensity relative to background, as well as loss of the low wavenumber peaks. Spectroscopically, plagioclase that has been transformed to amorphous material (either by melting or as diaplectic glass) exhibits one broad peak reflecting the Si-O stretching vibration.

Micro-FTIR spectroscopy of individual plagioclase grains, both naturally and experimentally shocked, has an added complexity in that infrared spectra are orientation-sensitive, where peak positions and intensities of vibrational modes in plagioclase can shift by ~40 wavenumbers, depending on orientation, making it difficult to correlate changes in peak intensities or positions with shock level (Fig. 9). However, the degree to which orientation affects the spectra decreases with increasing shock level (Jaret et al., 2018). Furthermore, orientation effects have been found to be a useful tool for distinguishing between diaplectic and melt-produced glasses. Diaplectic glass retains orientation effects in IR, despite its amorphous nature. Melt glass on the other hand does not show effects of orientation on spectral position.

5.5. Cathodoluminescence (CL)

The main effects of shock metamorphism on cathodoluminescence (CL) spectra of plagioclase are 1) decreasing luminescence with increasing amorphization (e.g., Fig. 12, Kaus and Bischoff, 2000; Götte, 2009; Götze, 2009; Pittarello et al., 2015; Kayama et al., 2018; Pittarello et al., 2020b); 2) the normal band emission at ~ 550-570 nm is often shifted to ~ 630 nm (Kayama et al., 2009a); 3) diaplectic plagioclase glass produces a broad band around 350 nm (Götte, 2009; Pittarello et al., 2015; Gucsik et al., 2004). Intriguingly, and in contrast to plagioclase, alkali feldspar shows increased CL intensity with increasing shock pressure (Kayama et al., 2012).

CL spectral analysis has been proposed to quantify shock effects and correlate with pressure (e.g., Kayama et al., 2012, 2018). However, the correlation between shock and signal intensity is complex because the intensity of the luminescent centers is regulated by numerous variables, including the abundance of activators, which can be trace elements, point defects, or both, and the abundance of quenchers, which would reduce the effect of the activators. Even in unshocked feldspars, the nature of activators is not always clear, so imaging studies must be accompanied by detailed back-scattered electron imaging in order to properly interpret the microstructures (e.g., Finch and Klein, 1999; Götze et al., 2000; Parsons et al., 2015). As a result of the complex mechanisms involved in luminescence, and therefore the relationship between luminescence and shock intensity, CL is generally viewed as less reliable than other techniques (e.g., XRD or Raman) for quantifying shock intensity, though it remains one of the most useful tools for investigating microstructures.

5.6. Raman spectroscopy

Raman spectroscopy allows identification of high-pressure phases (Section 3.9) and spectra show that increased shock corresponds to a progressive decrease in peak intensity and increase in peak width compared to unshocked feldspar (Fig. 13, e.g., Fritz et al., 2005b; Jaret et al., 2014). Peak positions and width are somewhat dependent on composition, so it is challenging to identify quantitative metrics in Raman spectra that uniquely identify shock.

At pressures < 29 GPa, shocked plagioclase has lower intensity and broader FWHM of characteristic Raman bands compared to unshocked plagioclase. At higher pressure ($>\sim 40$ GPa) Raman spectra exhibit a broad plateau as a result of amorphization (Fig. 13, Jaret et al., 2018). At much higher pressure (>45 GPa) high post-shock temperatures lead to recrystallization, and reappearance of the characteristic Raman spectra (Fritz et al., 2005a,b).

5.7. Photoluminescence spectroscopy

Photoluminescence spectroscopy is a technique, complementary to Raman spectroscopy, which has only been applied to shocked plagioclase by Pittarello et al. (2020b). Photoluminescence allows quantification of the “damage” in the lattice (i.e., amorphization) as percent of disordered structure within the investigated volume (a few μm^3). Similar to peak broadening in Raman spectra, Nd^{3+} luminescence bands get wider and are less defined with increased levels of amorphization.

5.8. Nuclear Magnetic Resonance (NMR) Spectroscopy

NMR spectroscopy uses nuclear spin transitions as a measure of the local chemical bonding and coordination environment (Stebbins and Xue, 2014). Because NMR is sensitive to the entire local chemical environment and not just long-range ordering, NMR is particularly useful for measuring the structure of amorphous materials. In amorphous silicates, NMR spectra of ^{29}Si ("^{29}Si NMR") are sensitive to the number and length of Si-O bonds, types of nearest neighbor atoms, and coordination of Si – all of which can change during shock deformation or if high-pressure phases are produced (Jaret et al., 2015).

6. Ongoing debates

6.1. Formation mechanism of diaplectic glass

The details of diaplectic glass formation are the subject of much debate. There are, in general, two main hypotheses: 1) rapid quenching of monomineralic melt at high pressure, or 2) solid-state structural collapse/destruction of atomic ordering of the mineral. Some details of these two formation hypotheses are explained here.

6.1.1. Melt formation

Grady (1977) interpreted diaplectic glass to form by quenching of a high-density melt phase upon pressure release. Such a phase would have solidified so rapidly that flow, which would normally erase the morphology and texture of the precursor minerals, did not have time to occur. In this scenario, local temperature spikes due to heterogeneous shock compression, cause local melting despite the temperature in the majority of the rock remaining below the liquidus (Grady et al., 1975; Grady, 1980). A key aspect of Grady's scenario for formation of diaplectic glass is the dissipation of strain energy by the development of shear bands. Microstructures similar to shear bands have been observed in recovered samples from rapid compression experiments (Sims et al., 2019). Similarly, Arndt et al. (1982) suggested that diaplectic glass forms from shock-induced melting, but that the duration of high temperature is short enough that the liquid transition is incomplete and the disordered transitional state is 'locked in'. Stöffler and Langenhorst (1994) explained the formation of diaplectic quartz glass by shock melting and quenching during decompression. The concept of diaplectic glass being a high-pressure melt was later adopted to explain the formation of maskelynite by Chen and El Goresy (2000) and El Goresy et al. (2013).

6.1.2. Solid state formation

The amorphous structure, and absence of flow textures, suggests a near instantaneous change from a crystalline structure to glass without melting (e.g., De Carli and Jamieson, 1959; Engelhardt and Stöffler, 1968). Ahrens et al. (1969) used shock experiments on plagioclase to suggest that diaplectic glass forms by solid-state release from a high-pressure phase during decompression. Williams and Jeanloz (1988) also favored a scenario where diaplectic glass is produced by reversion from a higher-pressure phase, which, similar to the scenario of Hemley et al. (1988), calls for high pressure-induced high-coordinated glasses. Hemley et al.'s assumption of a high-coordinated phase during shock compression rests on the experimentally determined Hugoniot curve where the steeper high-pressure branch (region III in Fig. 2) indicates a density during shock compression similar to the density expected of a compressed hollandite-like structured phase (Ahrens et al., 1969). A hollandite-like structure scenario would be supported by the existence of high-pressure phases and/or high-coordinated glasses. However, evidence of high-pressure phases was not observed in static experimentally produced diaplectic glass (Daniel et al., 1997; Sims et al., 2020). Likewise, high-coordinated glasses were not observed in in situ compression experiments or naturally shocked samples (Kubo et al., 2010; Jaret et al., 2015;

Sims et al., 2019). Furthermore, recent ^{29}Si NMR studies of natural diaplectic plagioclase, did not detect structural remnants of high-pressure high-coordination glass, even though such remnants would be resolvable with NMR analyses (Jaret et al., 2015). Ashworth and Schneider (1985) proposed a mechanism for diaplectic SiO_2 glass that is similar to metamictization – a process in which alpha particles physically displace atoms within the unit cell. In a diaplectic glass, physical displacement of atoms would be caused by the shock wave, rather than alpha particles.

Shock recovery experiments at starting temperatures of 77-293 K showed that in this temperature range the formation of diaplectic plagioclase glass is controlled by shock pressure only, and not temperature (Fritz et al., 2019a). This observation, together with the structural properties of diaplectic plagioclase glass (Jaret et al., 2015) and the recognition that diaplectic glass forms via a gradual collapse of the lattice (Hörz and Quaide, 1973, Fritz et al., 2019a), and the observation of isotropic twins alternating with crystalline twins in plagioclase (e.g., Stöffler, 1971; Pickersgill et al., 2015a,b; Pittarello et al., 2020a) further advocates for a solid-state amorphization mechanism.

6.2. Maskelynite and diaplectic glass

The first description of maskelynite was by Tschermak (1872) in the Shergotty martian meteorite, described as a previously unrecognised isotropic phase of near labradorite composition. This new phase was then named after M. H. N. Story-Maskelyne, a famous English mineralogist of the time. Tschermak (1883) then found the same phase in chondrites and, upon realizing that it was pseudomorphous with plagioclase, changed his interpretation to a melted or otherwise vitrified glass of plagioclase composition. A shock origin for maskelynite was suggested by Binns (1967) based on differences in the RI of maskelynite and melt-glass. At the same time, the term *diaplectic glass* was proposed to refer to “amorphous phases produced by shock waves without melting, and [which] are distinguishable from ordinary molten glasses” (Engelhardt et al., 1967; and Engelhardt and Stöffler, 1968). Since that time, *maskelynite* and *diaplectic plagioclase glass* have often been used interchangeably, which attached a genetic connotation to maskelynite. Historically, most isotropic plagioclase-composition material was called maskelynite, but modern observations have enabled us to distinguish between phases that have flowed (e.g., Chen and El Goresy, 2000) and “true” diaplectic glasses that show no evidence of melting (e.g., Jaret et al., 2015, Diemann and Arndt, 1984), even within a single thin section. Because there is confusion over how the term maskelynite is interpreted, it is imperative that clear observations regarding the nature of the isotropic phase be included in any description so that it is clear whether the authors are using “maskelynite” to refer to an apparently solid-state glass or a melt product.

7. Concluding remarks & remaining questions

Feldspars are typically difficult to study due to the optical complexity of their crystal structure and, when in the presence of water, their relatively rapid weathering rate. Consequently, the feldspar group is often neglected in favor of quartz or olivine for use in shock barometry. As a result, the shock scale for feldspar is limited and, essentially, qualitative. However, feldspars will have particular utility when studying quartz-poor rocks such as basalt, a dominant rock type on Mars and Earth’s moon, and an important surficial lithology on most terrestrial bodies. There have been many advances on the effects of shock metamorphism on feldspars over the past five decades but there are several major questions remain open, in particular:

1. Determining the exact nature and formation mechanism of diaplectic glass. Recent work has made significant strides, but confirmation and further studies would help to bolster these results (Section 6.1);
2. Understanding the formation of PDFs in feldspars, including exactly why the An content appears to be a controlling factor; the relationship between thin closely spaced shock-induced microtwins and PDFs; whether FFs form in feldspars; and the development of apparently shock-induced planar features that do not appear to be strict PDFs when investigated using high resolution TEM and EBSD (Section 3.4);
3. Whether or not measuring the crystallographic orientations of shock-induced planar features in feldspars can be improved upon and developed into a useful tool for shock barometry (Section 5.1);
4. Understanding the exact mechanism by which only alternate twins deform in polysynthetically twinned plagioclase, leaving the other set apparently undamaged, and whether this could be used to determine the local orientation of shock wave propagation (Section 3.6);
5. How, or if, the intensity of shock effects is affected by the presence of pre-existing microstructures (e.g., cleavage, twinning, exsolution), the crystallographic orientation with respect to the shock wave, and the presence of other mineral phases (Sections 3.4, 3.6);
6. How best to utilize and integrate multiple analytical techniques, which probe slightly different aspects of feldspar composition/structure and deformation (Section 5);

7. How to reconcile the pressure conditions associated with crystallographic transformations between various experimental techniques and naturally shocked materials, which is an ongoing challenge in many fields of geoscience: do all types of minerals behave in the same way during shock recovery experiments and natural impacts or do some mineral develop the same shock effects at lower pressures? (Section 4)
8. How does shock influence radioisotopic age determination? A topic not touched upon in this paper, because it is worth an entire volume on its own, but the interested reader can examine, for example, Jessberger and Ostertag (1982) and Fernandes et al. (2009).

Because shocked feldspars are a significant constituent of most planetary materials, the importance of understanding their shock behavior and ability to inform shock barometry will only become more relevant as we gain increasing numbers of samples from other planetary bodies.

8. ACKNOWLEDGMENTS

AEP is supported by the Leverhulme Trust Research Project Grant number RPG-2018-061. LP was supported by the Austrian Science Fund (FWF), project number V505-N29. JF thanks Vera Assis Fernandes and Ansgar Greshake for intense cooperation regarding the shock metamorphic record in meteorites and products of experiments. We thank E. L. Walton and J. G. Spray for thorough and helpful reviews.

9. REFERENCES CITED

Agarwal, A., Reznik, B., Kontny, A., Heissler, S., and Schilling, F., 2016, Lingunite-a high-pressure plagioclase polymorph at mineral interfaces in doleritic rock of the Lockne impact structure (Sweden): Scientific Reports, v. 6, p. 25991, doi:10.1038/srep25991.

Ahrens, T.J., Petersen, C.F., and Rosenberg, J.T., 1969, Shock compression of feldspars: Journal of Geophysical Research, v. 74, p. 2727–2746.

Ahrens, T.J., O'Keefe, J.D., and Gibbons, R. V, 1973, Shock compression of a recrystallized anorthositic rock from Apollo 15*: Proceedings of the 4th Lunar Science Conference, v. 3, p. 2575–2590.

Angel, R., 1988, High-pressure structure of anorthite: The American mineralogist, v. 73, p. 1114–1119.

Angel, R.J., 1994, Feldspars at High Pressure BT - Feldspars and their Reactions, in Parsons, I. ed., Dordrecht, Springer Netherlands, p. 271–312, doi:10.1007/978-94-011-1106-5_7.

Arndt, J., Hummel, W., and Gonzalez-Cabeza, I., 1982, Diaplectic labradorite glass from the Manicouagan impact crater; I, Physical properties, crystallization, structural and genetic implications: Physics and Chemistry of Minerals, v. 8, p. 230–239.

Ashworth, J.R., and Schneider, H., 1985, Deformation and transformation in experimentally shock-loaded quartz: Physics and Chemistry of Minerals, v. 11, p. 241–249, doi:10.1007/BF00307401.

Beck, P., Gillet, P., Gautron, L., Daniel, I., and El Goresy, A., 2004, A new natural high-pressure (Na,Ca)-hexaluminosilicate [(CaxNa1-x)Al3+xSi3-xO11] in shocked Martian meteorites: Earth and Planetary Science Letters, v. 219, p. 1–12, doi.org/10.1016/S0012-821X(03)00695-2.

Binns, R.A., 1967, Stony meteorites bearing maskelynite: Nature, v. 213, p. 1111–1112.

Bischoff, A., and Stöffler, D., 1984, Chemical and structural changes induced by thermal annealing of shocked feldspar inclusions in impact melt rocks from Lappajaervi Crater, Finland (W. V Boynton & G. Schubert, Eds.): Journal of Geophysical Research, v. 89, Suppl., p. 645–656, doi:http://dx.doi.org/10.1029/JB089iS02p0B645.

Bischoff, A., Schleiting, M., and Patzek, M., 2019, Shock stage distribution of 2280 ordinary chondrites—Can bulk chondrites with a shock stage of S6 exist as individual rocks? Meteoritics and Planetary Science, v. 54, p. 2189–2202, doi:10.1111/maps.13208.

Bowling, T.J., Johnson, B.C., Wiggins, S.E., Walton, E.L. , Melosh, H.J. Sharp, T.G., 2020, Dwell time at high pressure of meteorites during impact ejection from Mars: Icarus, 343, 113689, doi.org/10.1016/j.icarus.2020.113689.

Bunch, T.E., Cohen, A.J., and Dence, M.R., 1967, Natural terrestrial maskelynite: American Mineralogist, v. 52, p. 244–253.

Chen, M., and El Goresy, A., 2000, The nature of maskelynite in shocked meteorites; not diaplectic glass but a glass quenched from shock-induced dense melt at high pressures: Earth and Planetary Science Letters, v. 179, p. 489–502.

Chen, M., Sharp, T.G., El Goresy, A., Wopenka, B., and Xie, X., 1996, The majorite-pyrope + magnesiowüstite assemblage: Constraints on the history of shock veins in chondrites: Science, v. 271, p. 1570–1573, doi:10.1126/science.271.5255.1570.

Dachille, F., Gigl, P., and Simons, P.Y., 1968, Experimental and analytical studies of crystalline damage useful for the recognition of impact structures, in French, B.M. and Short, N.M. eds., Shock metamorphism of natural materials, Baltimore, MD, Mono Book Corp., p. 555–570.

Daniel, I., Gillet, P., McMillan, P.F., Wolf, G., and Verhelst, M.A., 1997, High-pressure behavior of anorthite: Compression and amorphization: Journal of Geophysical Research: Solid Earth, v. 102, p. 10313–10325, doi:10.1029/97jb00398.

Davison, T. M., Collins, G. S., and Ciesla, F. J., 2010, Numerical modelling of heating in porous planetesimal collisions: Icarus, v. 208, p. 468-481.

De Carli, P.S., and Jamieson, J.C., 1959, Formation of an amorphous form of quartz under shock conditions: The Journal of Chemical Physics, v. 31, p. 1675–1676, doi:10.1063/1.1730673.

Deer, W.A., Howie, R.A., and Zussman, J., 2001, Rock-forming minerals, Volume 4a: Framework silicates - Feldspars: London, The Geological Society, 972 p.

Dence, M. R., Douglas, J. A. V., Plant, A. G., and Traill, R. J., 1970, Petrology, Mineralogy, and deformation of Apollo 11 samples: Proceedings of the Apollo 11 Lunar Science Conference, v. 1, p 315-340.

Diemann, E., and Arndt, J., 1984, Diaplectic Labradorite Glass from the Manicouagan Impact Crater: II. X-Ray Diffraction Studies and Structural Model: Physics and Chemistry of Minerals, v. 11, p. 178-181.

Doeglas, D.J., 1940, Reliable and rapid method for distinguishing quartz and untwinned feldspar with the universal stage: American Mineralogist, v. 25, p. 286.

Dressler, B., 1990, Shock metamorphic features and their zoning and orientation in the Precambrian rocks of the Manicouagan Structure, Quebec, Canada: Tectonophysics, v. 171, p. 229–245, doi:10.1016/0040-1951(90)90101-D.

Dworak, U., 1969, Stoßwellenmetamorphose des Anorthosits vom Manicouagan Krater, Quebec, Canada: Contributions to Mineralogy and Petrology, v. 24, p. 306–347.

El Goresy, A., Chen, M., Gillet, P., and Dubrovinsky, L.S., 2000, Shock-induced high-pressure phase-transition of labradorite to hollandite "(Na47-Ca51-K2)" in Zagami and the assemblage hollandite "(Na80-Ca12-K8)" + jadeite in L chondrites: constraints to peak-shock pressures (D. W. G. Sears et al., Eds.): Meteoritics & Planetary Science, v. 35, p. A51–A51.

El Goresy, A., Gillet, P., Miyahara, M., Ohtani, E., Ozawa, S., Beck, P., and Montagnac, G., 2013, Shock-induced deformation of Shergottites: Shock-pressures and perturbations of magmatic ages on Mars: Geochimica et Cosmochimica Acta, v. 101, p. 233–262, doi:10.1016/j.gca.2012.10.002.

Engelhardt, W. von, and Bertsch, W., 1969, Shock induced planar deformation structures in quartz from the ries crater, Germany: Contributions to Mineralogy and Petrology, v. 21, p. 378, doi:10.1007/BF02672809.

Engelhardt, W. von, and Stöffler, D., 1968, Stages of shock metamorphism in crystalline rocks of the Ries Basin, Germany., in French, B.M. and Short, N.M. eds., Shock metamorphism of natural materials, Baltimore, MD, Mono Book Corp., p. 159–168.

Engelhardt, W. von, Arndt, J., Stöffler, D., Muller, W.F., Jeziorkowski, H., and Gubser, R., 1967, Diaplektische Gläser in den Breccien des Ries yon Nördlingen als Anzeichen für Stosswellenmetamorphose: Contributions to Mineralogy and Petrology, v. 15, p. 93–102.

Engelhardt, W. von, Arndt, J., Mueller, W.F., and Stöffler, D., 1970, Shock metamorphism of lunar rocks and origin of the regolith at the Apollo 11 landing site: Proceedings of the Apollo 11 Lunar Science Conference, v. 1, p. 363-384.

Evans, W.J., Yoo, C.S., Lee, G.W., Cynn, H., Lipp, M.J., and Visbeck, K., 2007, Dynamic diamond anvil cell (dDAC): A novel device for studying the dynamic-pressure properties of materials: Review of Scientific Instruments, v. 78, doi:10.1063/1.2751409.

Fairbairn, H.W., and Podolsky, T., 1951, Notes on precision and accuracy of optic angle determination with the universal stage: American Mineralogist, v. 36, p. 823.

Fernandes, V.A., Burgess, R., and Morris, A., 2009, ^{40}Ar-^{39}Ar age determinations of lunar basalt meteorites Asuka 881757, Yamato 793169, Miller Range 05035, LaPaz Icefield 02205, Northwest Africa 479, and basaltic breccia Elephant Moraine 96008: Meteoritics & Planetary Science, v. 44, p. 805–821. doi.org/10.1111/j.1945-5100.2009.tb00770.x.

Ferrière, L., and Osinski, G.R., 2013, Shock Metamorphism, in Osinski, G.R. and Pierazzo, E. eds., Impact Cratering: Processes and Products, Wiley-Blackwell, p. 106–124.

Ferrière, L., Morrow, J.R., Amgaa, T., and Koeberl, C., 2009, Systematic study of universal-stage measurements of planar deformation features in shocked quartz: Implications for statistical significance and representation of results: Meteoritics & Planetary Science, v. 44, p. 925–940.

Ferrière, L., Koeberl, C., Libowitzky, E., Reimold, W.U., Greshake, A., and Brandstätter, F., 2010, Ballen quartz and cristobalite in impactites: New investigations, in Gibson, R.L. and Reimold, W.U. eds., Large Meteorite Impacts and Planetary Evolution IV, Geological Society of America, v. 465, p. 0, doi:10.1130/2010.2465(29).

Finch, A.A., and Klein, J., 1999, The causes and petrological significance of cathodoluminescence emissions from alkali feldspars: Contributions to Mineralogy and Petrology, v. 135, p. 234–243, doi:10.1007/s004100050509.

Flemming, R.L., 2007, Micro X-ray diffraction (μXRD); a versatile technique for charcterization of Earth and planetary materials: Canadian Journal of Earth Sciences, v. 44, p. 1333–1346.

French, B.M., 1968, Sudbury structure, Ontario: Some petrographic evidence for an origin by meteorite impact, in French, B.M. and Short, N.M. eds., Shock metamorphism of natural materials, Baltimore, Mono Book Corp., p. 383–411.

French, B.M., 1998, Traces of catastrophe, a handbook of shock-metamorphic effects in terrestrial meteorite impact structures: Houston, TX, USA, Lunar and Planetary Institute, 120 p.

French, B.M., and Koeberl, C., 2010, The convincing identification of terrestrial meteorite impact structures: What works, what doesn't, and why: Earth-Science Reviews, v. 98, p. 123–170, doi:10.1016/j.earscirev.2009.10.009.

French, B.M., and Short, N.M. (ed)., 1968, Shock metamorphism of natural materials (B. M. French & N. M. Short, Eds.): Baltimore, Mono Book Corp., 644 p.

French, B., Hartung, J., Short, N., and Dietz, R., 1970, Tenoumer Crater, Mauritania. Age and petrologic evidence for origin by meteorite impact: Journal of Geophysical Research, v. 75, p. 4396–4406, doi:10.1029/jb075i023p04396.

French, B.M., Koeberl, C., Gilmour, I., Shirey, S.B., Dons, J.A., and Naterstad, J., 1997, The Gardnos impact structure, Norway: Petrology and geochemistry of target rocks and impactites: Geochimica et Cosmochimica Acta, v. 61, p. 873–904, doi:10.1016/S0016-7037(96)00382-1.

French, B. M., Cordua, W. S., and Plescia, J. B., 2004, The Rock Elm meteorite impact structure, Wisconsin: Geology and shock-metamorphic effects in quartz: GSA Bulletin, v. 116, p. 200–218.

Fritz, J., Greshake, A., and Stöffler, D., 2005a, Micro-Raman spectroscopy of plagioclase and maskelynite in Martian meteorites: Evidence of progressive shock metamorphism: Antarctic Meteorite Research, v. 18, p. 96–116.

Fritz J., Artemieva N. A., and Greshake A., 2005b, Ejection of Martian meteorites: Meteoritics & Planetary Science, v. 40, p. 1393–1411.

Fritz, J., Wünnemann, K., Reimold, W.U., Meyer, C., and Hornemann, U., 2011, Shock experiments on quartz targets pre-cooled to 77 K: International Journal of Impact Engineering, v. 38, p. 440–445, doi:10.1016/j.ijimpeng.2010.10.014.

Fritz, J., Greshake, A., and Fernandes, V.A., 2017, Revising the shock classification of meteorites: Meteoritics and Planetary Science, v. 52, p. 1216–1232, doi:10.1111/maps.12845.

Fritz, J., Assis Fernandes, V., Greshake, A., Holzwarth, A., and Böttger, U., 2019a, On the formation of diaplectic glass: Shock and thermal experiments with plagioclase of different chemical compositions: Meteoritics and Planetary Science, v. 54, p. 1533–1547, doi:10.1111/maps.13289.

Fritz, J., Greshake, A., Klementova, M., Wirth, R., Palatinus, L., Assis Fernandes, V., Bottger, U., and Ferriere, L., 2019b, Donwilhelmsite, IMA 2018-113. . CNMNC Newsletter No. 47, February 2019, page 199: European Journal of Mineralogy, v. 31, p. 197–202.

Gibbons, R., and Ahrens, T., 1977, Effects of shock pressures on calcic plagioclase: Physics and Chemistry of Minerals, v. 1, p. 95–107.

Gibson, R.L., and Reimold, W.U., 2005, Shock pressure distribution in the Vredefort impact structure, South Africa, in Kenkmann, T., Hörz, F.P., and Deutsch, A. eds., Special Paper - Geological Society of America, Geological Society of America (GSA), Boulder, CO, v. 384, p. 329–349.

Gillet, P., Chen, M., Dubrovinsky, L., and El Goresy, A., 2000, Natural $NaAlSi_3O_8$-hollandite in the shocked sixiangkou meteorite: Science (New York, N.Y.), v. 287, p. 1633–6.

Gillet, P., El Goresy, A., Beck, P., and Chen, M., 2007, High-pressure mineral assemblages in shocked meteorites and shocked terrestrial rocks: Mechanisms of phase transformations and constraints to pressure and temperature histories, in Ohtani, E. ed., Advances in High-Pressure Mineralogy, Geological Society of America, v. 421, p. 0, doi:10.1130/2007.2421(05).

Götte, T., 2009, Petrological modifications in continental target rocks from terrestrial impact structures: evidence from cathodoluminescence, in Gucsik, A. ed., Cathodoluminescence and its application in the planetary sciences, Heidelberg, Springer-Verlag, p. 45–60.

Götze, J., 2009, Cathodoluminescence microscopy and spectroscopy of lunar rocks and minerals BT - Cathodoluminescence and its application in the planetary sciences, *in* Gucsik, A. ed., Berlin, Heidelberg, Springer Berlin Heidelberg, p. 87–110, doi:10.1007/978-3-540-87529-1_5.

Götze, J., and Kempe, U., 2009, Physical principles of cathodoluminescence (CL) and its applications in geosciences, *in* Gucsik, A. ed., Physical principles of Cathodoluminescence (CL) and its applications in geosciences, Berlin, Springer-Verlag, p. 1–22.

Götze, J., Krbetschek, M.R., Habermann, D., and Wolf, D., 2000, High-resolution cathodoluminescence studies of feldspar minerals BT - Cathodoluminescence *in* geosciences, in Pagel, M., Barbin, V., Blanc, P., and Ohnenstetter, D. eds., Berlin, Heidelberg, Springer Berlin Heidelberg, p. 245–270, doi:10.1007/978-3-662-04086-7_10.

Grady, D.E., 1977, Processes occurring in shock wave compression of rocks and minerals, *in* Manghnani, M.H. and Akimoto, S.I. eds., High-pressure research: Applications in Geophysics, New York, Academic Press, p. 389–438.

Grady, D.E., 1980, Shock deformation of brittle solids: Journal of Geophysical Research, v. 85, p. 913–924, doi:http://dx.doi.org/10.1029/JB085iB02p00913.

Grady, D.E., and Murri, W.J., 1976, Dynamic unloading in shock compressed feldspar: Geophysical Research Letters, v. 3, p. 472–474.

Grady, D.E., Murri, W.J., and De Carli, P.S., 1975, Hugoniot sound velocities and phase transformations in two silicates: Journal of Geophysical Research, v. 80, p. 4857–4861, doi:http://dx.doi.org/10.1029/JB080i035p04857.

Gratz, A.J., Nellis, W.J., Christie, J.M., Brocious, W., Swegle, J., and Cordier, P., 1992, Shock metamorphism of quartz with initial temperatures -170 to + 1000°C: Physics and Chemistry of Minerals, v. 19, p. 267–288, doi:10.1007/BF00204005.

Grieve, R.A.F., 1975, Petrology and chemistry of the impact melt at Mistastin Lake crater, Labrador: Geological Society of America Bulletin, v. 86, p. 1617–1629.

Gucsik, A., Ninagawa, K., Nishido, H., Toyoda, S., Tsuchiyama, A., Bidló, A., and Brezsnyánszky, K., 2004, Cathodoluminescence (CL) spectral study of experimentally shock-deformed plagioclase, *in* Workshop on Chondrites and Protoplanetary Disk, Houston, TX, United States (USA), Lunar and Planetary Institute, Houston, TX, p. Abstract #9012.

Haff, J.C., 1940, Use of the Wulff net in mineral determination with the Universal stage: American Mineralogist, v. 24, p. 689–707.

Harris, R., Schultz, P., and Jaret, S., 2019, Critical comparison of textures observed in impact melt and volcanic rocks: Geological Society of America Abstracts with Programs, doi:10.1130/abs/2019AM-338073.

Hemley, R.J., Jephcoat, A.P., Mao, H.K., Ming, L.C., and Manghnani, M.H., 1988, Pressure-induced amorphization of crystalline silica: Nature, v. 334, p. 52–54, doi:10.1038/334052a0.

Hörz, F., 1968, Statistical measurements of deformation structures and refractive indices in experimentally shock loaded quartz, *in* French, B.M. and Short, N.M. eds., Shock metamorphism of natural materials, Baltimore, MD, Mono Book Corp., p. 243–253.

Hörz, F., and Quaide, W.L., 1973, Debye-Scherrer investigations of experimentally shocked silicates: The Moon, v. 6, p. 45–82.

Huffman, A.R., and Reimold, W.U., 1996, Experimental constraints on shock-induced microstructures in naturally deformed silicates: Tectonophysics, v. 256, p. 165–217, doi:10.1016/0040-1951(95)00162-x.

Huffman, A.R., Brown, J.M., Carter, N.L., and Reimold, W.U., 1993, The microstructural response of quartz and feldspar under shock loading at variable temperatures: Journal of Geophysical Research, v. 98, p. 22171–22197, doi:10.1029/93JB01425.

Iiishi, K.T., Tomisaka, T., Kato, T., and Umegaki, Y., 1971, Isomorphous substitution and infrared and far infrared spectra of the feldspar group: Neues Jahrbuch fuer Mineralogie. Abhandlungen, v. 115, p. 98–119.

Irifune, T., Ringwood, A. E., and Hibberson, W. O., 1994, Subduction of continental crust and terrigenous and pelagic sediments: an experimental study: Earth and Planetary Science Letters, v. 126, p. 351-368.

James, O.B., 1969, Jadeite: Shock-induced formation from oligoclase, Ries Crater, Germany: Science, v. 165, p. 1005 LP – 1008, doi:10.1126/science.165.3897.1005.

Janssen, C., Wirth, R., Rybacki, E., Naumann, R., Kemnitz, H., Wenk, H.-R., and Dresen, G., 2010, Amorphous material in SAFOD core samples (San Andreas Fault): Evidence for crush-origin pseudotachylytes? Geophysical Research Letters, v. 37, doi:10.1029/2009GL040993.

Jaret, S.J., Kah, L.C., and Harris, R.S., 2014, Progressive deformation of feldspar recording low-barometry impact processes, Tenoumer impact structure, Mauritania: Meteoritics & Planetary Science, v. 49, p. 1007–1022, doi:10.1111/maps.12310.

Jaret, S.J., Woerner, W.R., Phillips, B.L., Ehm, L., Nekvasil, H., Wright, S.P., and Glotch, T.D., 2015, Maskelynite formation via solid-state transformation: Evidence of infrared and X-ray anisotropy: Journal of Geophysical Research : Planets, v. 120, p. 570-587.

Jaret, S.J., Johnson, J.R., Sims, M., DiFrancesco, N., and Glotch, T.D., 2018, Microspectroscopic and petrographic comparison of experimentally shocked albite, andesine, and bytownite: Journal of Geophysical Research: Planets, v. 123, p. 1701–1722, doi:10.1029/2018JE005523.

Jessberger, E., and Ostertag, R., 1982, Shock-effects on the K-Ar system of plagioclase feldspar and the age of anorthosite inclusions from North-Eastern Minnesota: Geochimica et Cosmocimica Acta, v. 46, p. 1465 – 1471.

Johnson, J.R., 2003, Visible/near-infrared spectra of experimentally shocked plagioclase feldspars: Journal of Geophysical Research, v. 108, p. 5120, doi:10.1029/2003JE002127.

Johnson, J.R., Hörz, F., Lucey, P.G., and Christensen, P.R., 2002a, Thermal infrared spectroscopy of experimentally shocked anorthosite and pyroxenite; implications for remote sensing of Mars: Journal of Geophysical Research, v. 107, p. 14, doi:http://dx.doi.org/10.1029/2001JE001517.

Johnson, J.R., Staid, M.I., and Titus, T.N., 2002b, Shocked plagioclase signatures in thermal emission spectrometer data of Mars: Abstracts of Papers Submitted to the Lunar and Planetary Science Conference, v. 33, p. 0-Abstract 1345.

Johnson, J.R., Hörz, F., and Staid, M.I., 2003, Thermal infrared spectroscopy and modeling of experimentally shocked plagioclase feldspars: American Mineralogist, v. 88, p. 1575–1582.

Kaus, A., and Bischoff, A., 2000, Cathodoluminescence (CL) properties of shocked plagioclase: Meteoritics & Planetary Science, v. 35, p. A86.

Kayama, M., Gucsik, A., Nishido, H., Ninagawa, K., Tsuchiyama, A., and Goetze, J., 2009a, Cathodoluminescence and Raman spectroscopic characterization of experimentally shocked plagioclase: LPI Contribution, p. 49.

Kayama, M., Nakazato, T., Nishido, H., Ninagawa, K., Gucsik, A., and Goetze, J., 2009b, Cathodoluminescence characterization of maskelynite and alkali feldspar in shergottite: LPI Contribution, p. 50.

Kayama, M., Nishido, H., Ninagawa, K., Gucsik, A., and Goetze, J., 2009c, Cathodoluminescence of shocked plagioclase and alkali feldspar from Ries Crater, Germany: LPI Contribution, p. 51.

Kayama, M., Nishido, H., Sekine, T., Nakazato, T., Gucsik, A., and Ninagawa, K., 2012, Shock barometer using cathodoluminescence of alkali feldspar: Journal of Geophysical Research, v. 117, p. E09004.

Kayama, M., Sekine, T., Tomioka, N., Nishido, H., Kato, Y., Ninagawa, K., Kobayashi, T., and Yamaguchi, A., 2018, Cathodoluminescence of high-pressure feldspar minerals as a shock barometer: Meteoritics and Planetary Science, v. 53, p. 1476–1488, doi:10.1111/maps.13092.

Kieffer, S.W., 1971, Shock metamorphism of the Coconino sandstone at Meteor Crater, Arizona: Journal of Geophysical Research, v. 76, p. 5449–5473.

Kieffer, S.W., Schaal, R.B., Gibbons, R., Horz, R., Milton, D.J., and Dube, A., 1976, Shocked basalt from Lonar impact Crater, India, and experimental analogues: Lunar and Planetary Science Conference Proceedings, v. 1, p. 1391–1412.

Kleeman, J.D., 1971, Formation of diaplectic glass by experimental shock loading of orthoclase: Journal of Geophysical Research, v. 76, p. 5499–5503, doi:10.1029/JB076i023p05499.

Klein, C., and Philpotts, A., 2016, Introduction to mineralogy and petrology: Cambridge, Cambridge University Press.

Knight, K.S., Price G.D., 2008, Powder Neutron-diffraction studies of clinopyroxenes. I. The crystal structure and thermoelastic properties of jadeite between 1.5 and 270 K: The Canadian Mineralogist, v. 46, p. 1593–1622.

Koeberl, C., Reimold, W.U., Kracher, A., Träxler, B., Vormaier, A., and Körner, W., 1996, Mineralogical, petrological, and geochemical studies of drill core samples from the Manson impact structure, Iowa, *in* Koeberl, C. and Anderson, R.R. eds., The Manson impact structure, Iowa; anatomy of an impact crater, Geological Society of America, v. 302, p. 0, doi:10.1130/0-8137-2302-7.145.

Kubo, T., Kimura, M., Kato, T., Nishi, M., Tominaga, A., Kikegawa, T., and Funakoshi, K., 2010, Plagioclase breakdown as an indicator for shock conditions of meteorites: Nature Geoscience, v. 3, p. 41–45, doi:10.1038/NGEO704.

Kubo, T., Kono, M., Imamura, M., Kato, T., Uehara, S., Kondo, T., Higo, Y., Tange, Y., and Kikegawa, T., 2017, Formation of a metastable hollandite phase from amorphous plagioclase: A possible origin of lingunite in shocked chondritic meteorites: Physics of the Earth and Planetary Interiors, v. 272, p. 50–57, doi:10.1016/j.pepi.2017.09.006.

Lambert, P., 1979, Fractures induced by shock in quartz and feldspar: Mineralogical Magazine, v. 43, p. 527–533, doi:10.1180/minmag.1979.043.328.13.

Langenhorst, F., 2002, Shock metamorphism of some minerals: Basic introduction and microstructural observations: Bulletin of the Czech Geological Survey, v. 77, p. 265–282.

Langenhorst, F., and Deutsch, A., 1994, Shock experiments on pre-heated α- and β-quartz: I. Optical and density data: Earth and Planetary Science Letters, v. 125, p. 407–420, doi:10.1016/0012-821X(94)90229-1.

Langenhorst, F., and Deutsch, A., 2012, Shock metamorphism of minerals: Elements, v. 8, p. 31–36, doi:10.2113/gselements.8.1.31.

Langenhorst, F., and Dressler, B., 2003, First observation of silicate hollandite in a terrestrial rock: LPI Contribution, v. 1167, p. 0-Abstract 4046.

Langenhorst, F., and Poirier, J.-P., 2000, Anatomy of black veins in Zagami; clues to the formation of high-pressure phases: Earth and Planetary Science Letters, v. 184, p. 37–55, doi:http://dx.doi.org/10.1016/S0012-821X(00)00317-4.

Langenhorst, F., Deutsch, A., Stöffler, D., and Hornemann, U., 1992, Effect of temperature on shock metamorphism of single-crystal quartz: Nature, v. 356, p. 507–509, doi:10.1038/356507a0.

Langenhorst, F., Joreau, P., and Doukhan, J.C., 1995, Thermal and shock metamorphism of the Tenham chondrite: A TEM examination: Geochimica et Cosmochimica Acta, v. 59, p. 1835–1845, doi:10.1016/0016-7037(95)00086-F.

Lee, M.R., Parsons, I., Edwards, P.R., and Martin, R.W., 2007, Identification of cathodoluminescence activators in zoned alkali feldspars by hyperspectral imaging and electron-probe microanalysis: American Mineralogist, v. 92, p. 243–253, doi:10.2138/am.2007.2160.

Leichmann, J., Broska, I., and Zachovalová, K., 2003, Low-grade metamorphic alteration of feldspar minerals: A CL study: Terra Nova, v. 15, p. 104–108, doi:10.1046/j.1365-3121.2003.00467.x.

Letoullec, R., Pinceaux, J.P., and Loubeyre, P., 1988, The membrane diamond anvil cell: A new device for generating continuous pressure and temperature variations: high pressure research, v. 1, p. 77–90, doi:10.1080/08957958808202482.

Liu, L.-G., 1978, High-pressure phase transformations of albite, jadeite and nepheline: Earth and Planetary Science Letters, v. 37, p. 438–444, doi:10.1016/0012-821X(78)90059-6.

Liu, X., 2006, Phase relations in the system $KAlSi_3O_8$–$NaAlSi_3O_8$ at high pressure–high temperature conditions and their implication for the petrogenesis of lingunite: Earth and Planetary Science Letters, v. 246, p. 317-325.

Liu, L.-G., and El Gorsey, A., 2007, High-pressure phase transitions of the feldspars, and further characterization of lingunite: International Geology Review, v. 49, p. 854–860, doi:10.2747/0020-6814.49.9.854.

Lyon, R.J.P., 1963, Evaluation of infrared spectrophotometry for compositional analysis of lunar and planetary soils: NASA Technical Note D-1871.

Ma, C., Tschauner, O., Beckett, J.R., Liu, Y., Rossman, G.R., Zhuravlev, K., Prakapenka, V., Dera, P., and Taylor, L.A., 2015, Tissintite, (Ca,Na, ⊕)$AlSi_2O_6$, a highly-defective, shock-induced, high-pressure clinopyroxene in the Tissint martian meteorite: Earth and Planetary Science Letters, v. 422, p. 194–205, doi:10.1016/j.epsl.2015.03.057.

Ma, C., Tschauner, O. and Beckett, J.R., 2017, A new high-pressure calcium aluminosilicate ($CaAl_2Si_{3.5}O_{11}$) in martian meteorites: another after-life for plagioclase and connections to the CAS phase: Lunar and Planetary Science XLVIII, 1128.

Ma C., Tschauner, O., Beckett, J.R., Rossman G. R., Prescher C., Prakapenka, V.B. Bechtel, H. A., and MacDowell, A., 2018, Liebermannite, $KAlSi_3O_8$, a new shock-metamorphic, high-pressure mineral from the Zagami Martian meteorite: Meteoritics and Planetary Science, v. 53, p. 50-61.

Marsh, S. P. (Ed.), 1980, LASL shock Hugoniot data: University of California Press, Berkeley.

Melosh, H.J., 1989, Impact cratering: A geologic process: New York, Oxford University Press, 245 p.

Milton, D.J., and de Carli, P.S., 1963, Maskelynite: formation by explosive shock: Science, v. 140, p. 670 LP – 671, doi:10.1126/science.140.3567.670.

Moreau, J., Kohout, T., and Wünnemann, K., 2017, Shock-darkening in ordinary chondrites: Determination of the pressure-temperature conditions by shock physics mesoscale modeling: Meteoritics and Planetary Science, v. 52, p. 2375–2390, doi:10.1111/maps.12935.

Müller, W.F., and Hornemann, U., 1969, Shock-induced planar deformation structures in experimentally shock-loaded olivines and in olivines from chondritic meteorites: Earth and Planetary Science Letters, v. 7, p. 251–264, doi:10.1016/0012-821X(69)90062-4.

Myers, S.A., Cygan, R.T., Assink, R.A., and Boslough, M.B., 1998, ^{29}Si MAS NMR relaxation study of shocked Coconino Sandstone from Meteor Crater, Arizona: Physics and Chemistry of Minerals, v. 25, p. 313–317, doi:10.1007/s002690050120.

Nagy, S., Gucsik, A., Bérczi, S., Ninagawa, K., Nishido, H., Kereszturi, A., Hargitai, H., and Okumura, T., 2008, K-feldspar and biotite as shock indicator minerals from Bosumtwi impact crater: Abstracts of Papers Submitted to the Lunar and Planetary Science Conference, v. 39, Abstract 1144.

Nelson, S.T., and Montana, A., 1992, Sieve-textured plagioclase in volcanic rocks produced by rapid decompression: American Mineralogist, v. 77, p. 1242–1249.

Ogilvie, P., Gibson, R.L., Reimold, W.U., Deutsch, A., and Hornemann, U., 2011, Experimental investigation of shock metamorphic effects in a metapelitic granulite: The importance of shock impedance contrast between components: Meteoritics and Planetary Science, v. 46, p. 1565–1586, doi:10.1111/j.1945-5100.2011.01250.x.

Ohtani, E., Kimura, Y., Kimura, M., Takata, T., Kondo, T., and Kubo, T., 2004, Formation of high-pressure minerals in shocked L6 chondrite Yamato 791384: constraints on shock conditions and parent body size: Earth and Planetary Science Letters, v. 227, p. 505–515, doi:10.1016/j.epsl.2004.08.018.

Okuno, M., 2003, Structural evolution of quartz and feldspar crystals and their glasses by shock compression, *in* Davison, L., Horie, Y., and Sekine, T. eds., High-pressure shock compression of solids V. Shock wave and high pressure phenomena, New York.

Ostertag, R., 1982, Annealing behaviour of diaplectic plagioclase glass, *in* Lunar and Planetary Science Conference, p. 607–608.

Ostertag, R., 1983, Shock experiments on feldspar crystals: Journal of Geophysical Research, v. 88, Suppl., p. B364–B376, doi:10.1029/JB088iS01p0B364.

Papike, J.J., Taylor, L., and S., S., 1991, Lunar minerals, *in* Heiken, G.H., Vaniman, D., and French, B.M. eds., Lunar sourcebook: A user's guide to the Moon, Cambridge, Cambridge University Press, p. 736.

Parsons, I., and Lee, M.R., 2009, Mutual replacement reactions in alkali feldspars I: Microtextures and mechanisms: Contributions to Mineralogy and Petrology, v. 157, p. 641–661, doi:10.1007/s00410-008-0355-4.

Parsons, I., Steele, D.A., Lee, M.R., and Magee, C.W., 2008, Titanium as a cathodoluminescence activator in alkali feldspars: American Mineralogist, v. 93, p. 875–879, doi:10.2138/am.2008.2711.

Parsons, I., Gerald, J.D.F., and Lee, M.R., 2015, Routine characterization and interpretation of complex alkali feldspar intergrowths: American Mineralogist, v. 100, p. 1277–1303, doi:10.2138/am-2015-5094.

Pati, J.K., Jourdan, F., Armstrong, R.A., Reimold, W.U., and Prakash, K., 2010, First SHRIMP U-Pb and $^{40}Ar/^{39}Ar$ chronological results from impact melt breccia from the Paleoproterozoic Dhala impact structure, India, *in* Gibson, R.L. and Reimold, W.U. eds., Large Meteorite Impacts and Planetary Evolution IV, Geological Society of America, v. 465, doi:10.1130/2010.2465(27).

Pickersgill, A.E., and Lee, M.R., 2015, Identifying planar deformation features using EBSD and FIB, in Bridging the Gap III: Impact Cratering In Nature, Experiments, and Modeling, p. 1056.

Pickersgill, A.E., Flemming, R.L., and Osinski, G.R., 2015a, Toward quantification of strain-related mosaicity in shocked lunar and terrestrial plagioclase by in situ micro-X-ray diffraction: Meteoritics and Planetary Science, v. 50, p. 1851–1862, doi:10.1111/maps.12514.

Pickersgill, A.E., Osinski, G.R., and Flemming, R.L., 2015b, Shock effects in plagioclase feldspar from the Mistastin Lake impact structure, Canada: Meteoritics and Planetary Science, v. 50, p. 1546–1561, doi:10.1111/maps.12495.

Pickersgill, A.E., Lee, M.R., Daly, L., Mark, D.F., and IODP-ICDP Expedition 364 Science Party, 2017, Planar microstructures (lamellar subgrains) in feldspar from the Chicxulub impact structure, in 80th Annual Meeting of the Meteoritical Society, p. 6182.

Pittarello, L., and Koeberl, C., 2017, Shock-induced planar features in plagioclase: a project on measurements and investigations on their occurrence in relation with the An content, in 80th Annual Meeting of the Meteoritical Society.

Pittarello, L., Schulz, T., Koeberl, C., Hoffmann, J.E., and Münker, C., 2013, Petrography, geochemistry, and Hf-Nd isotope evolution of drill core samples and target rocks from the El'gygytgyn impact crater, NE Chukotka, Arctic Russia: Meteoritics and Planetary Science, v. 48, p. 1160–1198, doi:10.1111/maps.12088.

Pittarello, L., Roszjar, J., Mader, D., Debaille, V., Claeys, P., and Koeberl, C., 2015, Cathodoluminescence as a tool to discriminate impact melt, shocked and unshocked volcanics: A case study of samples from the El'gygytgyn impact structure: Meteoritics and Planetary Science, v. 50, p. 1954–1969, doi:10.1111/maps.12559.

Pittarello, L., Daly, L., Pickersgill, A.E., Ferrière, L., and Lee, M.R., 2020a, Shock metamorphism in plagioclase and selective amorphization: Meteoritics & Planetary Science, v. 55, p. 1103-1115, doi:10.1111/maps.13494

Pittarello, L., Fritz, J., Roszjar, J., Lenz, C., Chanmuang, C.N., and Koeberl, C., 2020b, Partial amorphization of experimentally shocked plagioclase: A spectroscopic study: Meteoritics and Planetary Science, v. 55, p. 669–678, doi:10.1111/maps.13445.

Pittarello, L., Ferrière, L., Feignon, J.-G., Osinski, G. R., and Koeberl, C., 2020c, Preferred orientation distribution of shock-induced planar microstructures in quartz and feldspar: Meteoritics & Planetary Science, v. 55, p. 1082-1092, doi: 10.1111/MAPS.13490-3304

Poelchau, M.H., and Kenkmann, T., 2011, Feather features; a low-shock-pressure indicator in quartz: Journal of Geophysical Research, v. 116, p. B02201, doi:http://dx.doi.org/10.1029/2010JB007803.

Poldervaart, A., and Gilkey, A.K., 1954, On clouded plagioclase: American Mineralogist, v. 35, p. 75–91.

Prior, D.J. et al., 1999, The application of electron backscatter diffraction and orientation contrast imaging in the SEM to textural problems in rocks: American Mineralogist, v. 84, p. 1741–1759, doi:10.2138/am-1999-11-1204.

Putnis, A., Hinrichs, R., Putnis, C. V., Golla-Schindler, U., and Collins, L.G., 2007, Hematite in porous red-clouded feldspars: Evidence of large-scale crustal fluid-rock interaction: Lithos, v. 95, p. 10–18, doi:10.1016/j.lithos.2006.07.004.

Reeder, R.J., and Michel, F.M., 2013, Application of total X-ray scattering methods and pair distribution function analysis for study of structure of biominerals, in Methods in Enzymology, doi:10.1016/B978-0-12-416617-2.00020-5.

Reimold, W.U., and Miller, R.M., 1989, The Roter Kamm impact crater, SWA/Namibia: Lunar and Planetary Science Conference Proceedings, v. 19, p. 711–732.

Reinhard, M., 1931, Universal Drehtischmethoden : Einführung in die kristalloptischen Grundbegriffe und die Plagioklasbestimmung: Basel, Verlag, von B. Wepf & Cie., 119 p.

Reynard, B., Okuno, M., Shimada, Y., Syono, Y., and Willaime, C., 1999, A Raman spectroscopic study of shock-wave densification of anorthite ($CaAl_2Si_2O_8$) glass: Physics and Chemistry of Minerals, v. 26, p. 432–436.

Ringwood, A.E., Reid, A.F., and Wadsley, A.D., 1967, High pressure transformation of alkali aluminosilicates and aluminogermanates: Earth and Planetary Science Letters, v. 3, p. 38–40, doi:http://dx.doi.org/10.1016/0012-821X(67)90008-8.

Robertson, P.B., 1973, Shock metamorphism of potassic feldspars: Durham University, 326 p.

Robertson, P.B., 1975, Experimental shock metamorphism of maximum microcline: Journal of Geophysical Research (1896-1977), v. 80, p. 1903–1910, doi:10.1029/JB080i014p01903.

Robertson, P.B., Dence, M.R., and Vos, M.A., 1968, Deformation in rock-forming minerals from Canadian craters, *in* French, B.M. and Short, N.M. eds., Shock metamorphism of natural materials, Baltimore, MD, Mono Book Corp., p. 433–452.

Roddy, D.J., Pepin, R.O., and Merrill, R.B. (Eds.), 1978, Impact and explosion cratering: Toronto, Pergamon Press, 1301 p.

Rubin, A.E., 1992, A shock-metamorphic model for silicate darkening and compositionally variable plagioclase in CK and ordinary chondrites: Geochimica et Cosmochimica Acta, v. 56, p. 1705–1714, doi:10.1016/0016-7037(92)90236-C.

Rucks, M.J., Whitaker, M.L., Glotch, T.D., Parise, J.B., Jaret, S.J., Catalano, T., and Dyar, M.D., 2018, Making tissintite: Mimicking meteorites in the multi-anvil: American Mineralogist, v. 103, p. 1516–1519, doi:10.2138/am-2018-6539.

Seifert, K.E., 1964, The genesis of plagioclase twinning in the Nonewaug Granite: The American Mineralogist, v. 49, p. 297–320.

Sharp, T.G., and DeCarli, P., 2006, Shock effects in meteorites, in Meteorites and the early solar system II, p. 653–677.

Sharp, T.G., Walton, E.L., Hu, J., Agee, C., 2019, Shock conditions recorded in NWA 8159 martian augite basalt with implications for the impact cratering history on Mars: Geochimica et Cosmochimica Acta, v. 246, p. 197-212.

Short, N.M., and Gold, D.P., 1996, Petrography of shocked rocks from the central peak at the Manson impact structure, *in* Koeberl, C. and Anderson, R.R. eds., Special Paper - Geological Society of America, Geological Society of America (GSA), Boulder, CO, v. 302, p. 245–265.

Sims, M. et al., 2019, Pressure-induced amorphization in plagioclase feldspars: A time-resolved powder diffraction study during rapid compression: Earth and Planetary Science Letters, v. 507, p. 166–174, doi:10.1016/j.epsl.2018.11.038.

Sims, M., Jaret, S.J., Johnson, J.R., Whitaker, M.L., and Glotch, T.D., 2020, Unconventional high-pressure Raman spectroscopy study of kinetic and peak pressure effects in plagioclase feldspars: Physics and Chemistry of Minerals, v. 47, p. 1–10, doi:10.1007/s00269-020-01080-z.

Smith, J. V, and Brown, W.L., 1988, Feldspar minerals: Berlin, Springer-Verlag, 828 p.

Spry, A.H., 1969, Metamorphic textures: Oxford, New York, Pergamon Press, 350

Stähle, V., Altherr, R., Nasdala, L., and Ludwig, T., 2011, Ca-rich majorite derived from high-temperature melt and thermally stressed hornblende in shock veins of crustal rocks from the Ries impact crater (Germany): Contributions to Mineralogy and Petrology, v. 161, p. 275–291, doi:10.1007/s00410-010-0531-1.

Stebbins, J.F., and Xue, X., 2014, NMR spectroscopy of inorganic Earth materials: Reviews in mineralogy and geochemistry, v. 78, p. 605–653, doi:10.2138/rmg.2014.78.15.

Stöffler D., 1966, Zones of Impact Metamorphism in the Crystalline Rocks of the Nördlinger Ries Crater: Contributions to Mineralogy and Petrology, v. 12, p. 15-24.

Stöffler, D., 1967, Deformation und Umwandlung von Plagioklas durch Stoßwellen in den Gesteinen des Nördlinger Ries: Contributions to Mineralogy and Petrology, v. 16, p. 51–83, doi:10.1007/BF00371608.

Stöffler, D., 1971, Progressive metamorphism and classification of shocked and brecciated crystalline rocks at impact craters: Journal of Geophysical Research, v. 76, p. 5541–5551.

Stöffler, D., 1972, Deformation and transformation of rock-forming minerals by natural and experimental shock processes: I. Behavior of minerals under shock compression: Fortschritte der Mineralogie, v. 49, p. 50–113.

Stöffler, D., 1974, Deformation and transformation of rock-forming minerals by natural and experimental shock processes: II. Physical properties of shocked minerals: Fortschritte der Mineralogie, v. 51, p. 256–289.

Stöffler, D., and Grieve, R.A.F., 2007, Impactites, *in* Fettes, D. and Desmons, J. eds., Metamorphic Rocks: A classification and glossary of terms, Recommendations of the International Union of Geological Sciences, Cambridge, UK, Cambridge University Press, p. 82–92, and 111–242.

Stöffler, D., and Hornemann, U., 1972, Quartz and feldspar glasses produced by natural and experimental shock: Meteoritics, v. 7, p. 371–394.

Stöffler, D., and Langenhorst, F., 1994, Shock metamorphism of quartz in nature and experiment: I. Basic observation and theory: Meteoritics, v. 29, p. 155–181.

Stöffler, D., Schulien, S., and Ostertag, R., 1975, Rock 61016: multiphase shock and crystallization history of a polymict troctolitic-anorthositic breccia: Lunar and Planetary Science Conference Proceedings, v. 1, p. 673–692.

Stöffler, D., Ostertag, R., Jammes, C., Pfannschmidt, G., Sen Gupta, P. R., Simon, S. B., Papike, J. J., and Beauchamp, R. H., 1986, Shock metamorphism and petrography of the Shergotty achondrite: Geochimica et Cosmochimica Acta v. 50, p. 889–903.

Stöffler, D., Keil, K., and Scott, E.R.D., 1991, Shock metamorphism of ordinary chondrites: Geochimica et Cosmochimica Acta, v. 55, p. 3845–3867, doi:http://dx.doi.org/10.1016/0016-7037(91)90078-J.

Stöffler, D., Hamann, C., and Metzler, K., 2018, Shock metamorphism of planetary silicate rocks and sediments: Proposal for an updated classification system: Meteoritics and Planetary Science, v. 53, p. 5–49, doi:10.1111/maps.12912.

Stöffler, D., Hamann, C., and Metzler, K., 2019, Addendum to "Stöffler, D., Hamann, C., and Metzler, K., Shock metamorphism of planetary silicate rocks and sediments: Proposal for an updated classification system. Meteoritics & Planetary Science 53, 5–49. Meteoritics & Planetary Science 54, 946-949. Stöffler, D., and Hornemann, U., 1972, Quartz and feldspar glasses produced by natural and experimental shock: Meteoritics, v. 7, p. 371–394.

Taylor, F.C., and Dence, M.R., 1969, A probable meteorite origin for Mistastin Lake, Labrador: Canadian Journal of Earth Sciences, v. 6, p. 39–45.

Thiel, M. van (Ed.), 1977, Compendium of shock wave data, (Livermore: Lawrence Livermore Laboratory Report UCRL-50108, 1977), p. 710-712.

Tomioka, N., and Miyahara, M., 2017, High-pressure minerals in shocked meteorites: Meteoritics and Planetary Science, v. 52, p. 2017–2039.

Tomioka, N., Mori, H., and Fujino, K., 2000, Shock-induced transition of NaAISi308 feldspar into a hollandite structure in a L6 chondrite: Geophysical Research Letters, v. 27, p. 3997–4000.

Tomioka et al., 2007, Static amorphization of plagioclase: Comparison to the formation pressure of diaplectic glass in shock experiments: Meteoritics and Planetarey Science, v. 42, p. A148

Tomioka, N., Kondo, H., Kunikata, A., and Nagai, T., 2010, Pressure-induced amorphization of albitic plagioclase in an externally heated diamond anvil cell: Geophysical Research Letters, v. 37, p. 1–5, doi:10.1029/2010GL044221.

Treiman, A., and Treado, P., 1998, Martian maskelynite? Raman spectra of plagioclase-composition glasses from ALH84001, EETA 79001, and ALHA 77005, in 29th Lunar and Planetary Science Conference, p. Abstract 1196.

Trepmann, C., Whitehead, J., and Spray, J., 2003, Shock effects in target rocks from the Charlevoix impact structure, Quebec, Canada: Abstracts of Geological Society of America Northeastern Section – 38th Annual Meeting, p. 7– 17.

Tschermak, G., 1883, Beitrag zur Klassifikation der Meteoriten: Sitzungsberichte der Mathematisch-Naturwissenschaftlichen Klasse der Kaiserlichen Akademie der Wissenschaften, Wien, v. 88, p. 347–371.

Tschermak, G., 1872, Die Meteoriten von Shergotty und Gopalpur: Sitzungsberichte der Mathematisch-Naturwissenschaftlichen Klasse der Kaiserlichen Akademie der Wissenschaften, Wien, v. 65, p. 122–145.

Turner, F.J., 1947, Determination of plagioclase with the four-axis universal stage: American Mineralogist, v. 32, p. 389–410.

Vernon, R.H., 1975, Deformation and recrystallization of a plagioclase grain: American Mineralogist, v. 60, p. 884–888.

Vinet, N., Flemming, R.L., and Higgins, M.D., 2011, Crystal structure, mosaicity, and strain analysis of Hawaiian olivines using in situ X-ray diffraction: American Mineralogist, v. 96, p. 486–497.

Wackerle, J., 1962, Shock-wave compression of quartz: Journal of Applied Physics, v. 33, p. 922, doi:10.1063/1.1777192.

Walawender, M.J., 1977, Shock-produced mosaicism in plagioclase, Charlevoix structure, Quebec: Canadian Journal of Earth Sciences = Revue Canadienne des Sciences de la Terre, v. 14, p. 74–81.

Walton, E.L., Sharp, T.G., Hu, J., and Filiberto, J., 2014 Heterogeneous mineral assemblages in martian meteorite Tissint as a result of a recent small impact event on Mars. Geochimica et Cosmochimica Acta. 140: 334-348

Walton, E.L., Sharp, T.G., Hu, J., 2016, Frictional melting processes and the generation of shock veins in terrestrial impact structures: Evidence from the Steen River impact structure, Alberta, Canada: Geochimica et Cosmochimica Acta, v. 180, p. 256-270.

White, J.C., 1993, Shock-induced amorphous textures in plagioclase, Manicouagan, Quebec, Canada: Contributions to Mineralogy and Petrology, v. 113, p. 524–532.

Whitehead, J., Grieve, R.A.F., and Spray, J.G., 2002, Mineralogy and petrology of melt rocks from the Popigai impact structure, Siberia: Meteoritics and Planetary Science, v. 37, p. 623–647, doi:10.1111/j.1945-5100.2002.tb00844.x.

Whitney, P.R., 1972, Spinel inclusions in plagioclase of metagabbros from the Adirondack Highlands: American Mineralogist, v. 57, p. 1429–1436.

Williams, Q., and Jeanloz, R., 1988, Spectroscopic evidence for pressure-induced coordination changes in silicate glasses and melts: Science, v. 239, p. 902 LP – 905, doi:10.1126/science.239.4842.902.

Wittmann, A., Korotev, R.L., Jolliff, B.L., Nishizumi, K., Jull, A.J.T., Caffee, M.W., Zanetti, M., Irving, A.J., 2019, Petrogenesis of lunar impact melt rock meteorite Oued Awlitis 001: Meteoritics and Planetary Science, v. 54, p. 2167-2188.

Xu, C., Zhao, S.R., Li, C., and He, X., 2016, Plagioclase twins in a basalt: An electron backscatter diffraction study: Journal of Applied Crystallography, v. 49, p. 2145–2154, doi:10.1107/S1600576716015739.

Yagi, A., Suzuki, T., and Akaogi, M., 1994, High pressure transitions in the system KAlSi3O8-NaAlSi3O8: Physics and Chemistry of Minerals, v. 21, p. 12–17.

Zoltai, T., and Stout, J.H., 1984, Mineralogy: concepts and principles: Minneapolis, Burgess Publishing Company, 505 p.

10. FIGURE CAPTIONS

Figure 1: Plot showing the relationship between anorthite content and pressure needed to form partly to fully isotropic plagioclase. The overall trend demonstrates that plagioclase of higher mole % An content results in complete amorphization at lower pressures than plagioclase of lower mole % An content. The graph is based on shock recovery experimental data summarized by Fritz et al. (2019a).

Figure 2: Shock pressure versus specific volume Hugoniot plot of a representative plagioclase ($An_{\sim 50}$) illustrating the three distinct phase regimes (I, low pressure; II, mixed; and

III, high pressure) and the range of the Hugoniot elastic limit (HEL). Data from Marsh (1980) and van Thiel (1977).

Figure 3: A) Transmitted light photomicrograph of heavily fractured anorthite in Apollo sample 15415,90; fractures are highlighted by offset twins when viewed between crossed polarizers. B) Backscattered electron image of fractured plagioclase (albite, dark grey) from the El'gygytgyn impact structure, with planar features (black arrows) in the lower right corner.

Figure 4: Undulatory extinction in Apollo samples 76335,55 (A) and 60215,13 (B) between cross-polarized light, as the stage is rotated a wave of extinction passes through the crystal.

Figure 5: Planar microstructures in oligoclase from the Tenoumer impact structure (A, B); note the planar features in (B) only exist in alternating twins; after Jaret et al. (2014). C) Andesine (An_{23}) from the Manicouagan impact structure showing multiple sets of planar features. D) K-rich feldspar with albite exsolution (beige, labeled Ab) and tartan twins spread over the whole grain from the Gardnos impact structure; planar features on the right side of the image (parallel to white lines) with the same orientation as polysynthetic twins.

Figure 6: Plane-polarised photomicrographs of andesine experimentally shocked to 25 GPa (A) and 56 GPa (B) showing progressive degrees of shock-darkening. Electron probe microanalysis, Raman, and FTIR analyses suggest this darkening is purely optical, and does not correspond with observable chemical or structural changes. After Jaret et al. (2018).

Figure 7: Diaplectic plagioclase glass. A) Illustration of maskelynite in the Shergotty martian meteorite, highlighting preserved external crystal morphology and irregular fractures extending from maskelynite grain margins into surrounding igneous pyroxene (after Tschermak 1872, drawn at 75x magnification, estimated grain size is ~400 μm). B) Composite reflected light (left) and transmitted light between crossed polarizers (right) image showing a partly isotropic plagioclase crystal enclosed by olivine in martian meteorite Chassigny, though the plagioclase is only partly isotropic, the same fracture pattern is observed as in the illustration by Tschermak (A). C,D) Partially isotropic plagioclase in PPL (C) and XPL (D) from Apollo 15 sample 15684,4. Black areas in XPL remain extinct on rotation of the stage. E,F) Completely isotropic plagioclase in basalt from Lonar crater, India (after Jaret et al. 2015). G) Plane-polarised transmitted light image of maskelynite from the Shergotty meteorite (~30 GPa) which includes a perfectly preserved magmatic pyroxene. H) Plane-polarised transmitted light image of maskelynite from the Los Angeles Martian meteorite (~45 GPa) with a pyroxene fragment partially affected by eutectic melting.

Figure 8: Plots demonstrating the relationship between refractive index, pressure, and composition of diaplectic feldspar glasses. A) Refractive index vs. An content. Displayed are isobars indicating the shock pressures that result in a plagioclase normative phase with a given index of refraction. Fields indicating the optical properties, birefringent or isotropic, are indicated by grey lines; after Fritz et al. (2005b) using data from Stöffler et al. (1986). B) Refractive indices of diaplectic feldspar glasses from experiments in the pressure range from 28-45 GPa. After Ostertag (1983).

Figure 9: IR spectra of 2 orientations from (A) crystalline, (B) diaplectic glass, and (C) melt glass of labradorite composition. Crystalline labradorite exhibits multiple peaks, all showing shifts with orientation indicating the anisotropic nature of the material. Both melt glass and diaplectic glass are amorphous (one broad peak) but diaplectic glass retains orientation effects not observed in the melt glass sample. After Jaret et al. (2015).

Figure 10: Plane-polarised light photomicrograph of plagioclase glass displaying bubbles and flow textures surrounded by brown stained olivine, in some areas the plagioclase glass has developed a rim of recrystallized plagioclase. From the strongly shocked ALH (Allan Hills) 77005 martian meteorite.

Figure 11: Photomicrographs of sieve or checkerboard feldspar. A, B) Plagioclase from Gow Lake impact structure, showing preserved polysynthetic twins between crossed polarizers (B). C) Plane-polarized light photomicrographs showing magnified view of checkerboard feldspar in a clast from Gow Lake impact melt rock; D) sieve-textured feldspar from a volcanic andesite (image credit: Dr Alessandro Mommio).

Figure 12: Cathodoluminescence images and spectra of plagioclase (An_{55}) experimentally shocked to 28 GPa by Fritz et al., (2019a). A) Transmitted light photomicrograph between crossed polarizers (XPL) showing heterogeneous distribution of isotropic domains (black). B) Optical microscope cathodoluminescence (OM-CL) image of the same grain as in (A), showing three spectra locations (1-3). Areas of higher crystallinity (point 1) have higher luminescence

than isotropic domains (points 2 and 3). C) CL spectra corresponding to points 1-3 in (B), further showing that the domains with remaining crystallinity have higher luminescence than those that are isotropic, after Pittarello et al. (2020b).

Figure 13: Raman spectra of shocked feldspar. A) Raman spectra of andesine (An_{43}): unshocked (0 GPa), shocked (up to 29 GPa), and diaplectic glass (>29 GPa). For clarity, three spectra of 0 GPa (top line), 26 GPa (middle line), and 56 GPa (bottom line), representing the aforementioned categories (unshocked, shocked, diaplectic glass) are shown here. Up to pressures of 29 GPa (middle line), increasing shock corresponds to an overall decrease in peak intensity and causes the 480/510 Δ cm^{-1} peak ratio to approach 1. Above 29 GPa (bottom line), the sample appears amorphous, and exhibits a different Raman pattern, with two broad peaks at ~500 Δ cm^{-1} and 580 Δ cm^{-1}. Data from Jaret et al. (2018). B) Raman spectra of diaplectic feldspar glass with three different An contents (top: An_{15} – naturally shocked L6 chondrite; middle: An_{50} – experimentally shocked troctolite; bottom: An_{94} – experimentally shocked gabbro). The spectral position of the hump in the region of 950 to 1150 cm^{-1} varies with An content. Data from Fritz et al. (2019a).

Table 1: Summary table of impact-related metamorphism in feldspar group minerals, with key to the section of the paper that discusses them in more detail (Column 1: "Sctn.") and relevant figures (Fig.). Reported pressures are in GPa and are derived from [1]Ostertag (1983) and [2]Jaret et al. (2018), both of which conducted shock recovery (gas gun) experiments. These pressures should act as guides and are indicative of trends in the order of formation of shock features, however the exact values may not be directly applicable to natural samples for reasons discussed in Section 4.

Sctn.	Feature	Fig.	Orthoclase	Sanidine	Microcline	Albite	Oligoclase	Andesine	Labradorite	Bytownite
			Single crystal[1]	Single crystal[1]	Single crystal[1]	An_{02}, rock [2]	Single crystal[1]	An_{43}, rock [2]	Single crystal[1]	An_{77} [b], rock[1], [2]
3.1	Irregular fracturing[a]	3	<10.5 to 32	<10.5 to 30	<10.5 to 34	*N.R.*	<10.5 to 29	*N.R.*	10.5 to 27	10.5 to 26[a]
3.2	Undulatory extinction	4								
	Wave of extinction passes through the grain		*No limits explicitly stated*							
3.3	Mosaicism	*b*								
	Patchwork of slightly different extinction angles within a grain		10.5 to 28	14 to 30	14 to 45	*Ambiguous*	~18 to 31	*Ambiguous*	18 to 28	22 to 27[1]
3.4	Planar features/microstructures	5								
	Open parallel planar fractures (PFs) and/or Closely spaced parallel planar lamellae (PDFs)		~10.5 to 36	10.5 to 31	~10.5 to 42	*N.O.*	~14 to 33	*N.O.*	14 to 23	14 to 27[1] N.O. [2]
3.5	Shock darkening	6								
	Darkening of mineral in plane-polarised transmitted light		*N.R.*	*N.R.*	*N.R.*	>~24	N.R.	>~24	*N.R.*	>~22[1]
3.7	Diaplectic glass	7								
	Amorphous phase that maintains external crystal form and internal features such as chemical zoning — Partial		>26-28	>26-28	>26-28	~50-56	~26-28	~28-30	>26-28	~25-27 [2]
	Complete		>32-34	>32-34	>45[c]	>~55 [d]	>32-34	>~47 [d]	>28-30	>28-30[1]; >~38 [2] [d]
3.8	Melt glass	10								
	Amorphous phase that shows flow textures and/or vesiculation		45-50 [e]	45-50 [e]	45-50 [e]	*N.O.*	>42 [e]	*N.O.*	>42 [e]	>45-50[1] [e]; N.O. [2]
3.9	High pressure phases									
	Phases related to feldspar composition that are stable at higher pressure conditions than found on Earth's surface		*See Table 2*							
3.10	Sieve and checkerboard feldspar	11								
	Feldspar clasts in melt rocks made up of individual rectangular domains separated by melt products		*Temperature rather than pressure is the controlling factor*							
3.6	Alternate twin deformation	5a,b								
	Special cases of planar features or diaplectic glass confined to only alternate twins		*This is a broad category of effects that each seem to occur over a narrow range of pressure conditions, somewhat lower than the equivalent full grain effect. e.g., alternate diaplectic glass twins fall into the category above of "partial isotropization".*							

N. R. = Not reported – features were not explicitly discussed in the manuscript so presence in those samples is ambiguous. **N.O.** = None observed - explicitly stated that the author looked but did not find that feature in the sample. **Ambiguous** = Jaret et al. (2018) found a texture reminiscent of mosaicism, but were ambiguous in their interpretation, so did not explicitly report pressure conditions for mosaicism in those samples. **[a]**Ostertag (1983) found that fracturing decreased over 22 GPa. **[b]**Note: no images of mosaicism are included because it is challenging to accurately capture that feature in a still image, and no high quality images were found. **[c]**Ostertag (1983) found that microcline maintained reduced birefringence up to 45 GPa, where their experiments stopped. **[d]**Note: Different pressures for the amorphisation of plagioclase are reported in the literature, the table shows data from Ostertag (1983) and Jaret et al. (2018) and Figure 1 uses the data compiled by Fritz et al. (2019a), as a result the values reported in this table for complete amorphisation from Jaret et al. (2018) are higher (~55 GPa, ~47 GPa, ~38 GPa) than those shown in

Figure 1 (<35 GPa), likely due to differences in experimental setup and/or plagioclase composition. [e]Ostertag (1983) did not detect melt glass unambiguously, so assumed values to be in accordance with Stöffler and Hornemann (1972).

Table 2: High-pressure phases commonly associated with feldspathic compositions in highly shocked lithologies, including name, chemical composition, type locality, and the experimentally derived stability fields. The pressure [P] stability field of high-pressure phases strongly depends on chemical composition of the environment, and the prevailing temperatures [T], so the presented P-T conditions serve only as a guide and further details can be found in the cited references.

Name	Formula	Type Locality	Synthesized	Meteorites	Terrestrial impact structures	P-T	Refs.
Donwilhelmsite	$CaAl_4Si_2O_{11}$	Lunar meteorite Oued Awlitis 001	Yes	Yes	No	13 – 36 GPa, >1200 °C	1-3
Jadeite	$NaAlSi_2O_6$	Myanmar		Yes	Yes	2.5 GPa; 1000 °C	4-9
Liebermannite (K-Hollandite)	$KAlSi_3O_8$	Martian meteorite Zagami	Yes			12 GPa, 1026 °C	10-16
Lingunite (Na-Hollandite)	$NaAlSi_3O_8$	Sixiangkou L6 chondrite	Yes	Yes	Yes	Stable at 22-23 GPa; >1200 °C Metastable at ~20-24 GPa; ~1100-1300 °C	11-15, 17-22
Tissintite	$(Ca,Na,\square)AlSi_2O_6$	Martian meteorite Tissint	Yes			6 - 8.5 GPa; 1000-1350 °C	23, 24
Zagamiite	$CaAl_2Si_{3.5}O_{11}$	Martian meteorite Zagami		Yes			23-26

[1] Fritz et al. (2019b), [2] Irifune et al. (1994), [3] Beck et al. (2004), [4] James (1969), [5] Ohtani et al. (2004), [6] Tomioka et al. (2007), [7] Knight and Price (2008), [8] Kubo et al. (2010), [9] Stähle et al. (2011), [10] Ringwood et al. (1967), [11] El Goresy et al. (2000), [12] Gillet et al. (2000), [13] Langenhorst and Poirier (2000), [14] Tomioka et al. (2000), [15] Langenhorst and Dressler (2003), [16] Ma et al. (2018), [17] Liu (1978), [18] Yagi et al. (1994), [19] Liu (2006), [20] Liu and El Goresy (2007), [21] Agarwal et al. (2016), [22] Kubo et al. (2017), [23] Ma et al. (2015), [24] Rucks et al. (2018), [25] Walton et al. (2014), [26] Ma et al. (2017).

Table 3: Summary of different experimental techniques for calibrating shock features and parameters.

Technique	Timescale	Method	Purpose	References
Shock	Nanoseconds	In situ measurements of shockwaves	Determination of the equation of state (EoS) using Rankine-Hugoniot relations (Fig. 2)	Wackerle (1962)
Shock recovery	Shock pulses of microsecond duration	Shock impedence or reverberation technique	Investigations of shock effects in materials Determination of phase stability	Müller and Hornemann (1969); Hörz and Quaide (1973); Fritz et al. (2011)
Rapid compression	Seconds – 10s mins	Membrane and dynamic diamond anvil cell	Determination of phase stability Typically collect simultaneous XRD during compression and decompression	Letoullec et al. (1988); Evans et al. (2007); Sims et al. (2019)
Static compression	Minutes to hours	Diamond anvil cell	Determination of phase stability Typically coupled with either XRD or Raman spectroscopy after each compression step	Angel (1988); Williams and Jeanloz (1988); Daniel et al. (1997); Sims et al. (2020)

Table 4: Summary of analytical techniques used for assessing shock in feldspars. Optical microscopy is not included as it is assumed that primary characterization has already been conducted.

Technique		Sample requirements	General technique use	Limitations	Application to studies of shock metamorphism	Refs.
Universal-stage (U-stage)		Thin section	Measuring 3D orientation of planar and linear elements (i.e., twins, PDFs, optic axes)	Complex operation for biaxial solid solution minerals like feldspars (see Section 5.1) Only possible to view about 2/3 of a rectangular thin section U-stage does not fit on most modern microscopes	Indexing planar microstructures	(1-4)
Electron Backscattered Diffraction (EBSD)		Highly polished surface (i.e., thin or thick section, polished mount) Crystalline material Sample must fit in SEM	Analysing the distribution of orientations within or between minerals Measuring deformation within a crystal Identifying phases	Cannot uniquely index planar features without the addition of U-stage measurements or FIB cross-sectioning (see Section 5.1) Only applicable to crystalline material (no patterns provided by amorphous material)	Indexing planar microstructures (Section 5.1, complementary to other techniques) Increasing internal misorientation with increasing shock pressure No diffraction from diaplectic and melt glasses	(5-8)
X-ray diffraction (XRD)	Powder	Powder (whole rock or mineral separates)	Identifying phases Quantifying strain Refining crystal structure Identifying lattice breakdown (e.g., evaluating degree of shock)	Cannot distinguish amorphous phases from each other	Peaks broaden in chi direction (single-crystal or in situ μXRD only) at relatively low pressure Peaks broaden in the 2θ direction at higher pressure No diffraction from diaplectic and melt glasses (they produce a broad diffuse band)	(9-12)
	Single-crystal	Individual mineral separate				
	In situ μxRD	Thin sections Polished mount Hand sample				
High-energy total X-ray scattering		Powdered mineral (~mg) Single crystal	Quantifying atomic distances and positions (e.g., evaluating degree of ordering)	Requires synchrotron beamtime	Diaplectic glasses show intermediate order but no long-range order and orientation effects Melt glasses show no ordering >10 Å and no orientation effects	(13-14)
Cathodoluminescence (CL)		Thin section Thick section Polished mount	Imaging microstructures and defects	Luminescence is controlled by multiple variables, such as the abundance of activators (trace elements, point defects, both), and the abundance of quenchers	Plagioclase: Normal band emission at ~550-570 nm commonly shifted to ~630 nm with increasing pressure Diaplectic glass results in a broad band ~ 350 nm Increasing amorphisation causes decreasing luminescence Alkali-feldspar: Increasing pressure results in increasing luminescence	(15-31)
Raman spectroscopy		Thin section Thick section Polished mount	Identifying phases (i.e., high-pressure polymorphs; see Section 3.9) Evaluating crystallinity	Libraries and databases for mineral identification are limited Difficult to assign individual peaks to specific modes	Bands progressively broaden and decrease in intensity resulting in increased FWHM with increasing pressure Diaplectic and melt glasses result in broad peaks about 500 and 1000 cm^{-1} (dependent on composition, see Fig. 14)	(31–36)
Photoluminescence spectroscopy		Thin section Thick section Polished mount	Revealing lattice defects	Need to have endmembers for quantitiative damage calibration (unshocked to completely amorphous)	Nd^{3+} luminescence bands broaden with increasing amorphization	(27)

Thermal infrared absorption spectroscopy	Powder (whole rock or mineral separates) (mgs – 10 mgs)	Identifying phases Measuring crystal lattice structure	Averages grain orientations, so no orientation effects are detectable Limited sensitivity to minor components of the mixture	Decreased spectral detail and intensity with increasing pressure Loss of low wavenumber peaks (as a result of lattice disordering and increased glass content) with increasing pressure Diaplectic and melt glass result in one broad peak	(14, 35, 37–44)
Micro FTIR spectroscopy	Thin section Thick section Polished mount		Orientation sensitive measurements (e.g., peak height) can be hard to match to databases of non-oriented measurements	Decreased intensity of peaks due to loss of crystallinity with increasing pressure Diaplectic glass preserves orientation effects Melt glass does not preserve orientation effects	(14, 35)
Nuclear magnetic resonance (NMR) spectroscopy	Powder (whole rock or mineral separates) (mgs – 10 mgs)	Identifying phases Determining local chemical environment	Sample must include an NMR active isotope (e.g., ^{29}Si in feldspars)	Diaplectic glass lacks long range order, results in a spectral shape similar to melt glass, but peak centre and FWHM are more similar to crystalline plagioclase Melt glass lacks long range order, and results in broader spectral peak than crystalline plagioclase or diaplectic plagioclase glass	(14, 45)

[1] Reinhard (1931), [2] Turner (1947), [3] Stöffler (1967), [4] Dworak (1969), [5] Prior et al. (1999), [6] Pickersgill et al. (2017), [7] Pickersgill and Lee (2015), [8] Pittarello et al. (2020a), [9] Hörz and Quaide (1973), [10] Flemming (2007), [11] Vinet et al. (2011), [12] Pickersgill et al. (2015a), [13] Reeder and Michel (2013), [14] Jaret et al. (2015), [15] Lee et al. (2007), [16] Parsons et al. (2008), [17] Parsons and Lee (2009), [18] Finch and Klein (1999), [19] Götze et al. (2000), [20] Parsons et al. (2015), [21] Kaus and Bischoff (2000), [22] Götte (2009), [23] Gucsik et al. (2004), [24] Götze (2009), [25] Pittarello et al. (2015), [26] Kayama et al. (2018), [27] Pittarello et al. (2020b), [28] Kayama et al. (2012), [29] Kayama et al. (2009a), [30] Kayama et al. (2009b), [31] Kayama et al. (2009c), [32] Fritz et al. (2005a), [33] Fritz et al. (2019a), [34] Jaret et al. (2014), [35] Jaret et al. (2018), [36] Reynard et al. (1999), [37] Lyon (1963), [38] Bunch et al. (1967), [39] Stöffler and Hornemann (1972), [40] Stöffler (1974), [41] Arndt et al. (1982), [42] Ostertag (1983), [43] Johnson et al. (2002a), [44] Johnson (2003), [45] Myers et al. (1998).

Table 5: Summary table of orientations of shock-induced planar microstructures in feldspars measured by U-stage.

Feldspar composition	Reported orientation(s)	Crater	References
Labradorite	(001), (010), (111), (203), (101)	Manicouagan	Dworak (1969)
Andesine (~An_{30})	(001) 25%, (010) 11%, (100) 10%, ($1\bar{2}0$) 10%, (012) 7%, (130) 6%, others occurring at less than 2% frequency	Ries	Stöffler (1967)
Plagioclase	(001), (010), ($\bar{1}02$), and ($1\bar{2}1$)	Several Canadian craters	Robertson et al. (1968)
An_{98}	(101), (010), (021)	Apollo breccia 10046	Dence et al. (1970)

Figure 1

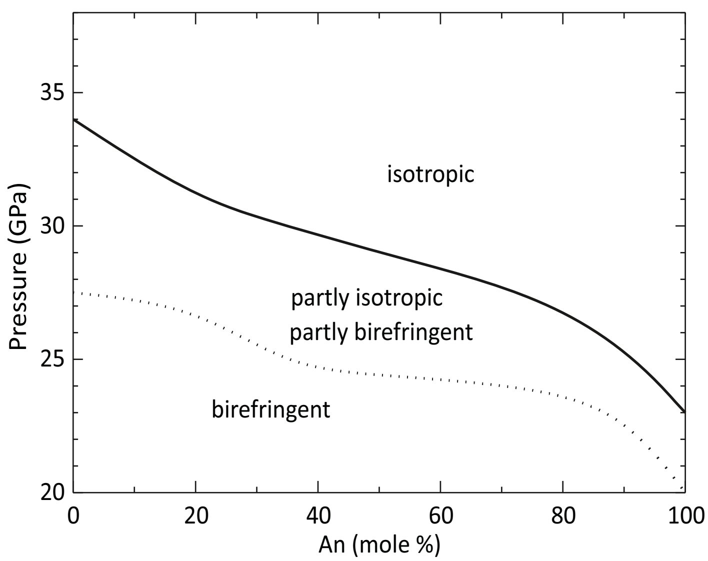
isotropic
partly isotropic
partly birefringent
birefringent
Pressure (GPa)
35
30
25
20
0
20
40
60
80
100
An (mole %)

Figure 2

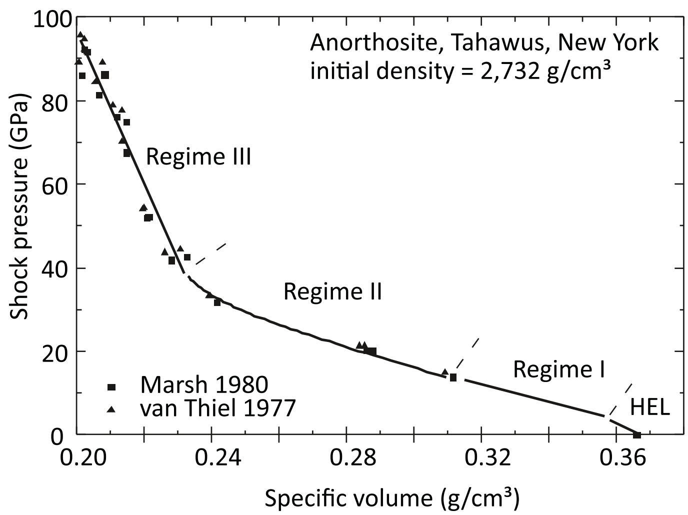

Anorthosite, Tahawus, New York
initial density = 2,732 g/cm³
Regime III
Regime II
Regime I
HEL
Marsh 1980
van Thiel 1977
Shock pressure (GPa)
Specific volume (g/cm³)
0
20
40
60
80
100
0.20
0.24
0.28
0.32
0.36

Figure 3

Figure 4

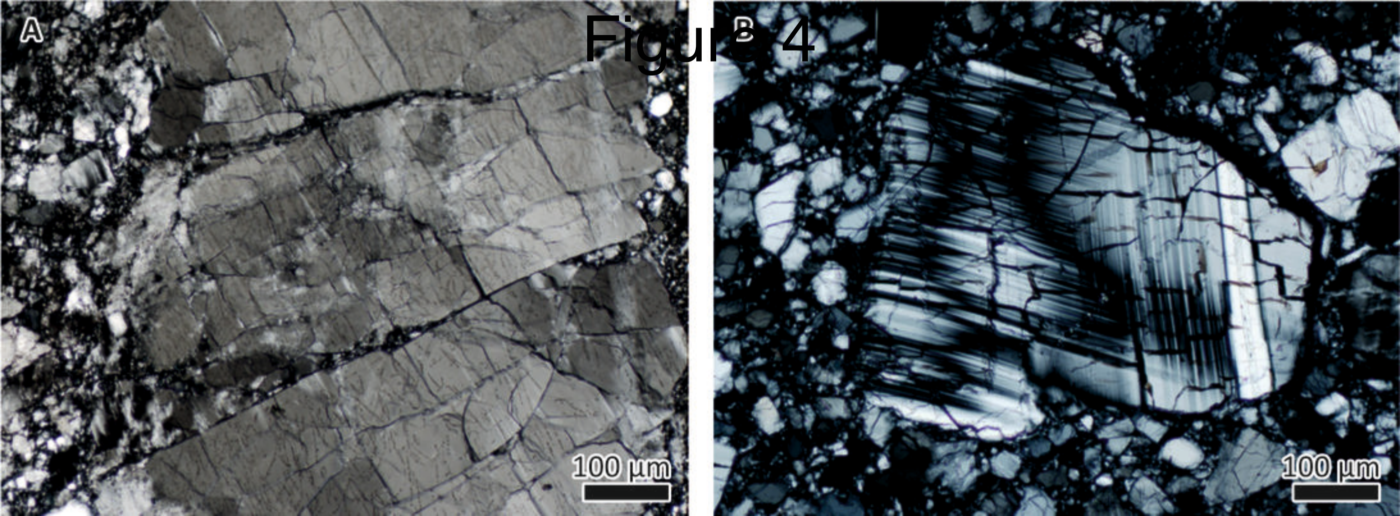

Figure 5

Figure 6

Figure 7

Figure 8

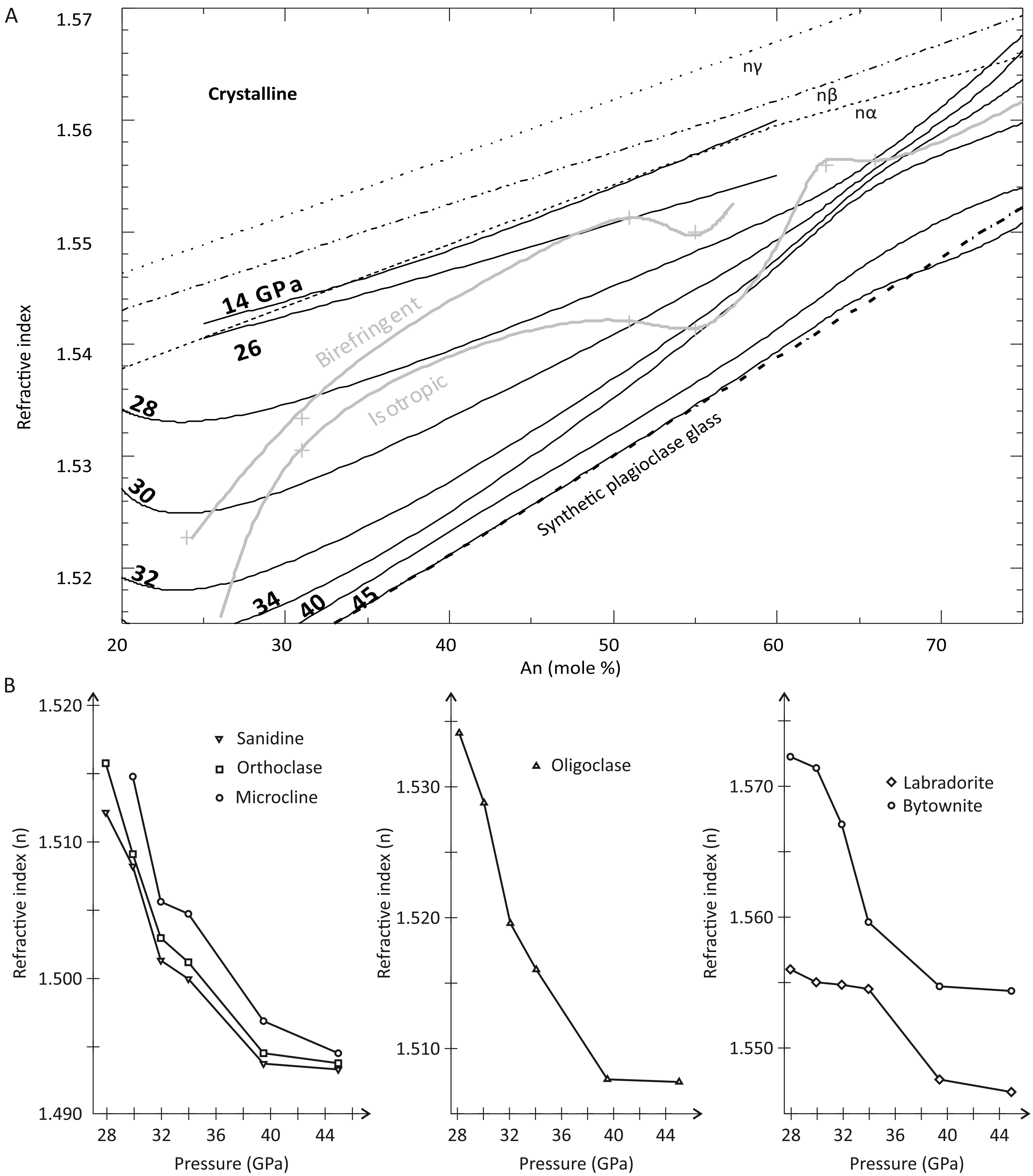
A
Crystalline
nγ
nβ
nα
14 GPa
26
28
30
32
34
40
45
Birefringent
Isotropic
Synthetic plagioclase glass
Refractive index
An (mole %)
B
Sanidine
Orthoclase
Microcline
Oligoclase
Labradorite
Bytownite
Refractive index (n)
Pressure (GPa)

Figure 9

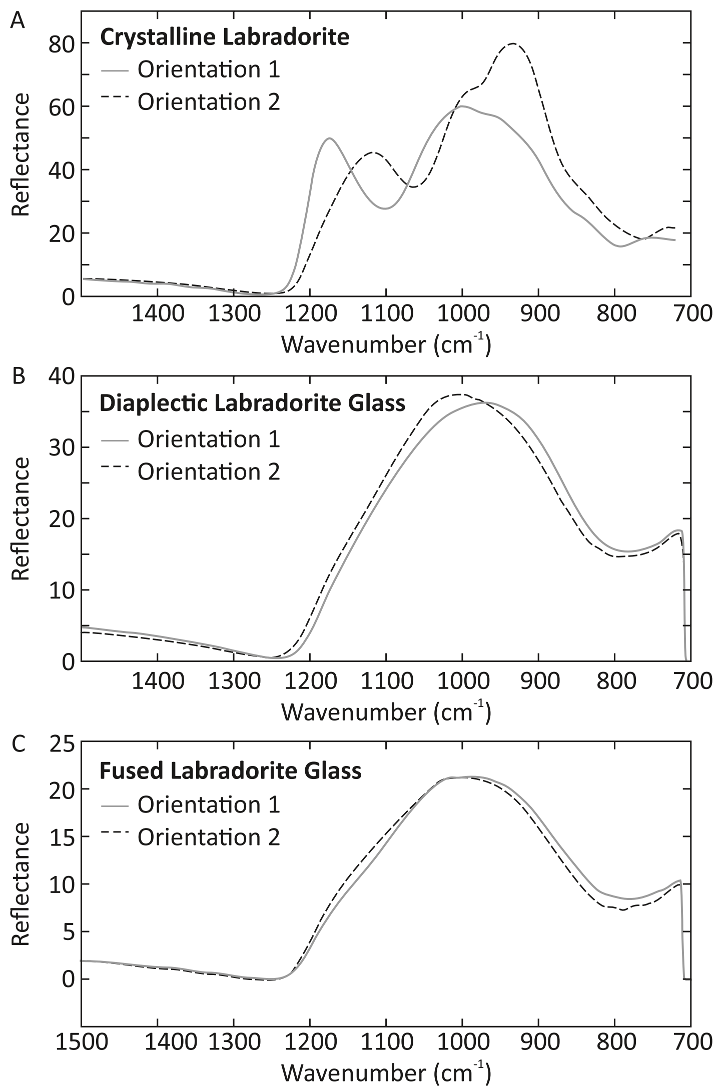
A
Crystalline Labradorite
Orientation 1
Orientation 2
Reflectance
80
60
40
20
0
1400
1300
1200
1100
1000
900
800
700
Wavenumber (cm-1)
B
Diaplectic Labradorite Glass
Orientation 1
Orientation 2
Reflectance
40
30
20
10
0
1400
1300
1200
1100
1000
900
800
700
Wavenumber (cm-1)
C
Fused Labradorite Glass
Orientation 1
Orientation 2
Reflectance
25
20
15
10
5
0
1500
1400
1300
1200
1100
1000
900
800
700
Wavenumber (cm-1)

Figure 10

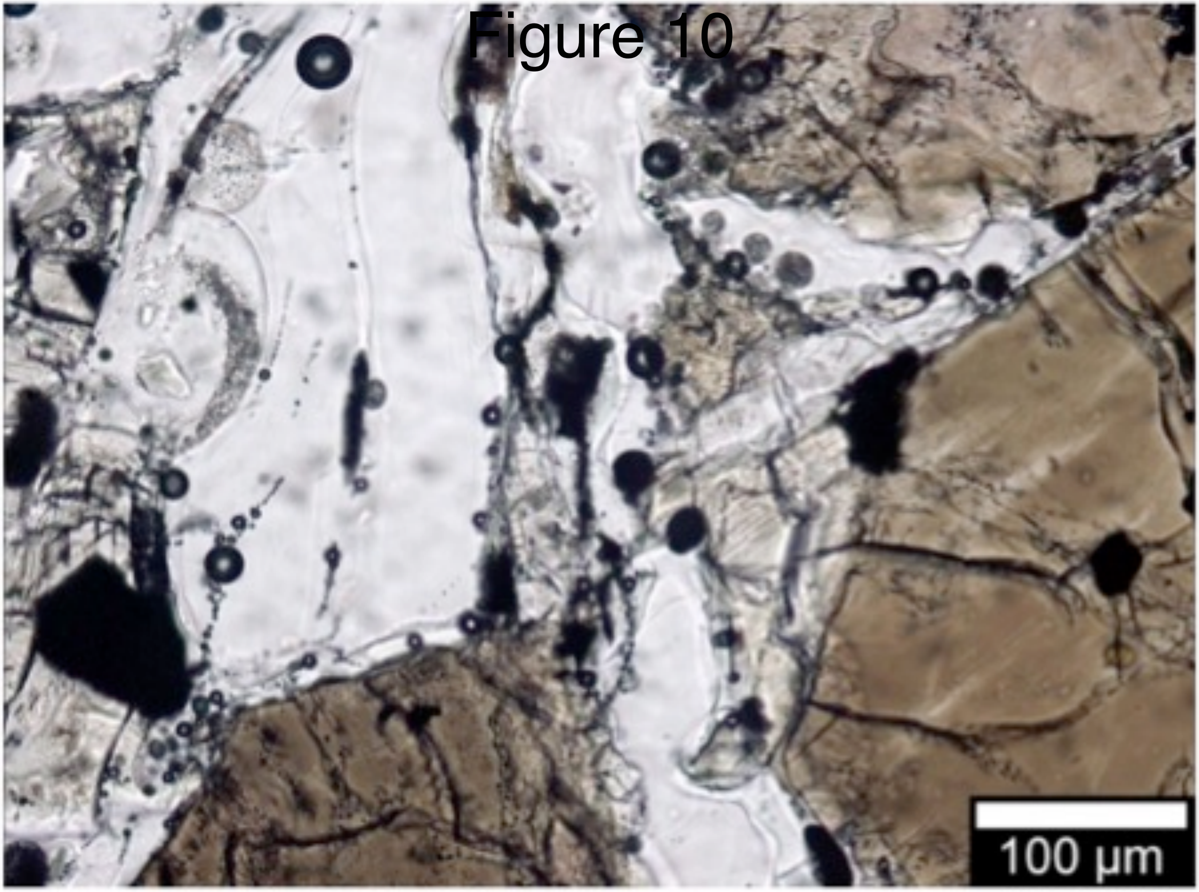

ure 11

Figure 12

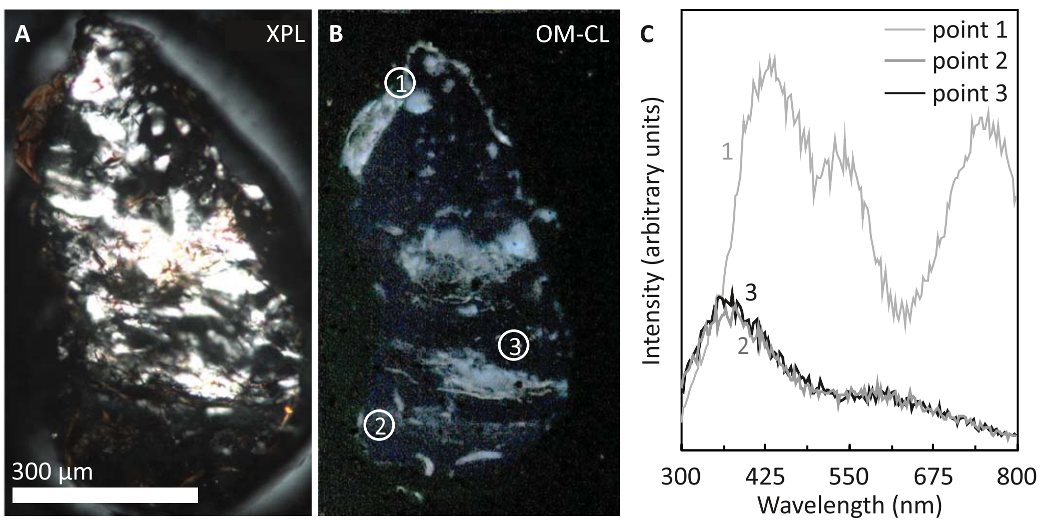
A
XPL
300 µm
B
OM-CL
1
2
3
C
point 1
point 2
point 3
Intensity (arbitrary units)
Wavelength (nm)
300
425
550
675
800

Figure 13

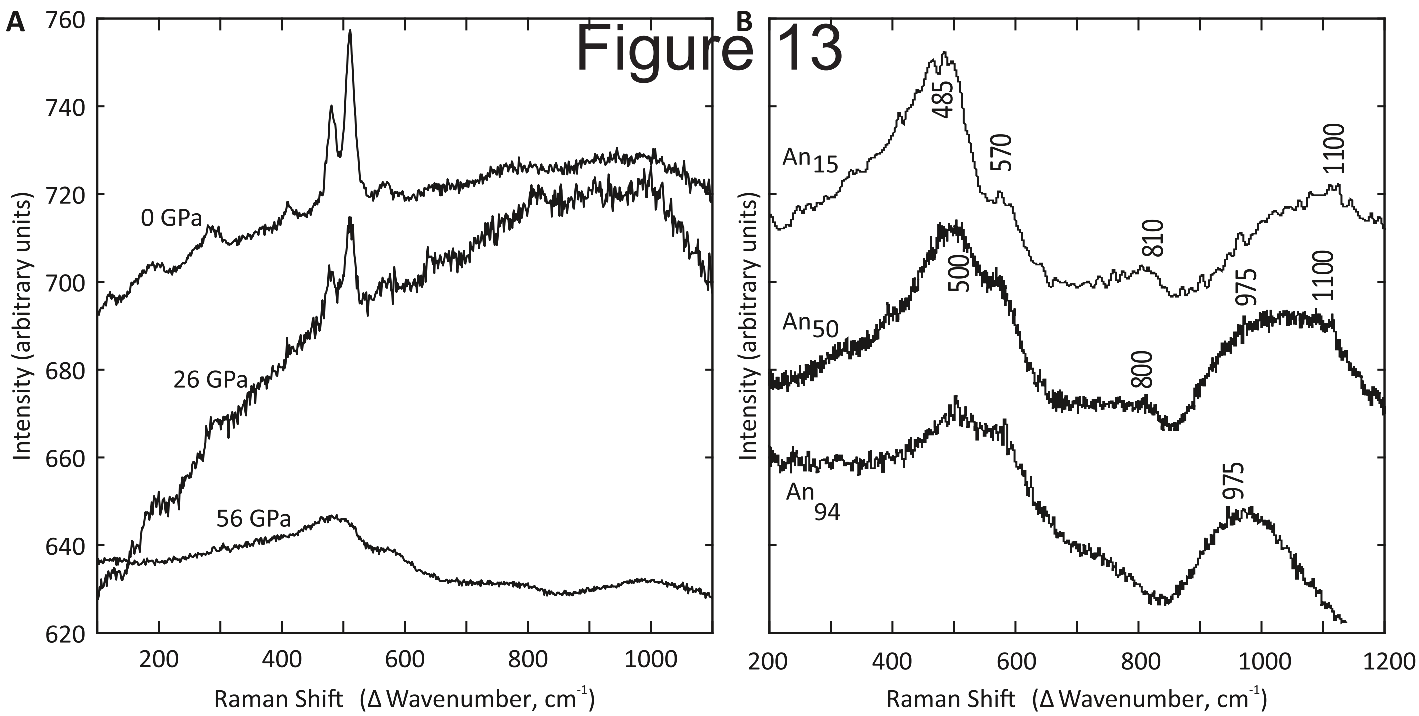
A
B
Figure 13
760
740
720
700
680
660
640
620
0 GPa
26 GPa
56 GPa
Intensity (arbitrary units)
200
400
600
800
1000
Raman Shift (Δ Wavenumber, cm-1)
An15
An50
An94
485
570
1100
810
500
975
1100
800
975
200
400
600
800
1000
1200
Intensity (arbitrary units)
Raman Shift (Δ Wavenumber, cm-1)